

11/17/03  
TD-03-054

# HFDC01 Test Summary

S. Feher, G. Ambrosio, N. Andreev, R. Carcagno, D. Chichili, V. Kashikin, M. Lamm, I. Novitski, D. Orris, Y. Pischalnikov, C. Sylvester, M. Tartaglia, J. Tompkins, R. Yamada, A.V. Zlobin

## Contents:

|  |    |
|--|----|
| 1. Introduction  | 1  |
| 2. Quench Testing  | 1  |
| 3. Temperature Margin Measurements and Spot Heater Studies | 12 |
| 4. Magnetic Measurements                                   | 17 |
| 5. Strain gauge results                                    | 25 |
| 6. AC loss Measurements                                    | 35 |
| 7. RRR measurement   | 36 |

# 1. Introduction

HFDC01 is a double aperture magnet utilizing coils with pan cake configuration. This magnet was completed in June, 2003. The magnet was installed into the VMTF dewar and it was electrically checked by August 3<sup>rd</sup>, 2003. The VMTF dewar was filled with liquid helium on August 8<sup>th</sup>. Since we cooled VMTF by using dewars, we finished testing the next day. We kept the magnet cold, however the temperature was gradually increasing and when we were able to resume testing in September 15<sup>th</sup> the temperature was close to 200 K. First test cycle of the magnet has been completed on September 24<sup>th</sup>. When the magnet was at room temperature we removed it from the VMTF dewar and re-adjusted its preloading. The second test cycle started on October 16<sup>th</sup>, 2003 and it was completed on October 23<sup>rd</sup>.

## 2. Quench Testing

Summary of the quenches are presented in Figure 1. Although the beginning of the training was promising, the magnet after the seventh quench exhibited very slow and erratic training. The magnet hasn't completed its training so it was hard to make any reasonable ramp rate or temperature dependence studies. In an attempt to speed up the training process we did try few higher ramp rate and lower temperature quenches but we observed no significant change of the quench current. Consequently from the quench history one can conclude that there was no indication of any ramp rate or temperature dependence. After each (intentional and unintentional) thermal cycles it seems the magnet experienced little re-training. On the other hand we haven't seen any improvement of the quench current between the two test cycles even if expected a change since we changed the preload of the coils.

### 2.1. Quench origins

In table I. we listed the quench start segments found with a software tool developed for finding voltage rises. The start time of a quench in a voltage tap segment was determined by tracing back the voltage rise in the segment to the last point  $2\sigma$  below the noise. Unfortunately the V-tap locations were not so frequent that we could use a time of flight technique to localize more precisely the quenches. Also, most of the time in more than one segments, which were relatively quite far apart from each other had quenches appeared. The maximum information one can extract from these events were to claim that the quench has started in a block of conductor. We can distinguish (based on V-taps locations) six blocks. In figure 2. we plotted the quench current history where the quenches were grouped together based on the block they were originated. On figure 3 quench training is plotted as a function of coil blocks. In figure 4. we plotted a typical quench event (quench #23).

### 2.2. Some unusual quenches

In figure 5. we plotted the voltage rises of several segments in quench #14. There is an obvious peculiarity to this event. The voltage rises of two adjacent segments which

share the same V-tap are quite unusual. Both signals have a swing to negative polarity which should mean that locally the current flow was reverse. If we make a hypothesis that the quench occurred right where the V-tap was located the developing resistance could act like a voltage divider. One can imagine to draw a special bridge type of circuit where the current flows according to the resistance distribution. If we add to the equation the fact that the resistance distribution can change due to the quench development we can explain the negative swing of the voltage rise.

From the phenomena described above one can draw an important conclusion: we will know indirectly the quench location, since in such a scenario the quench should have started right at the V-tap location. Since the V-tap was located at the end of the coil, it shows that the ends are probably not well supported. It is also interesting to mention that it is very probable that the turn below the last turn was also quenching, since the segment next to the turn to which this voltage tap was attached, was also quenching about the same time.

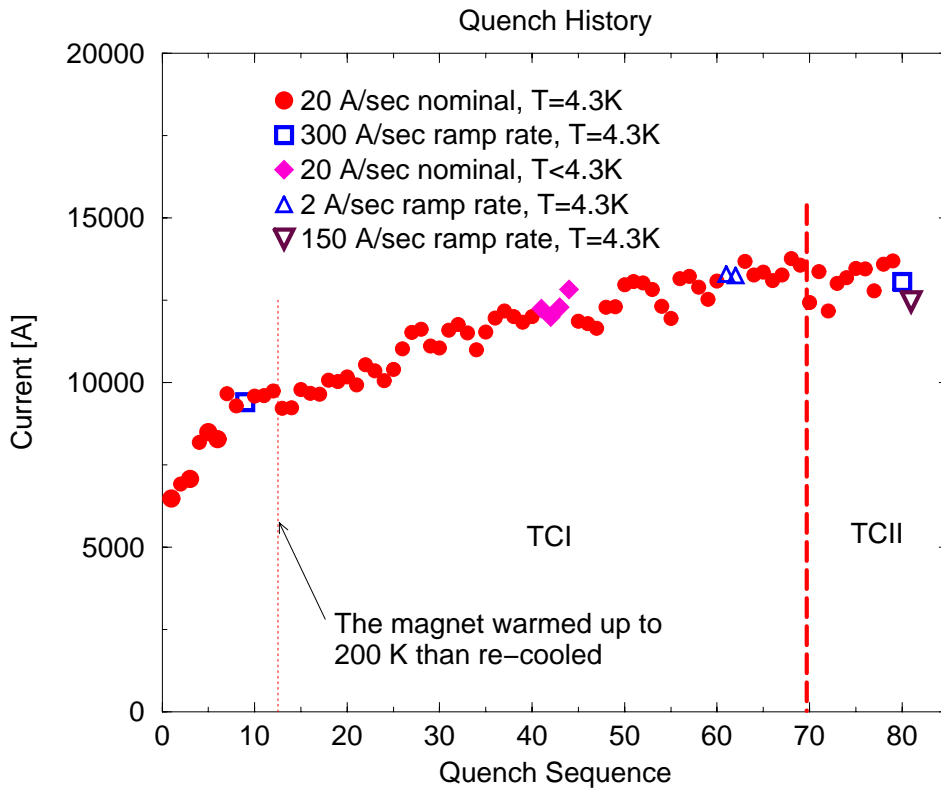


Figure 1. Quench history of HFDC01.

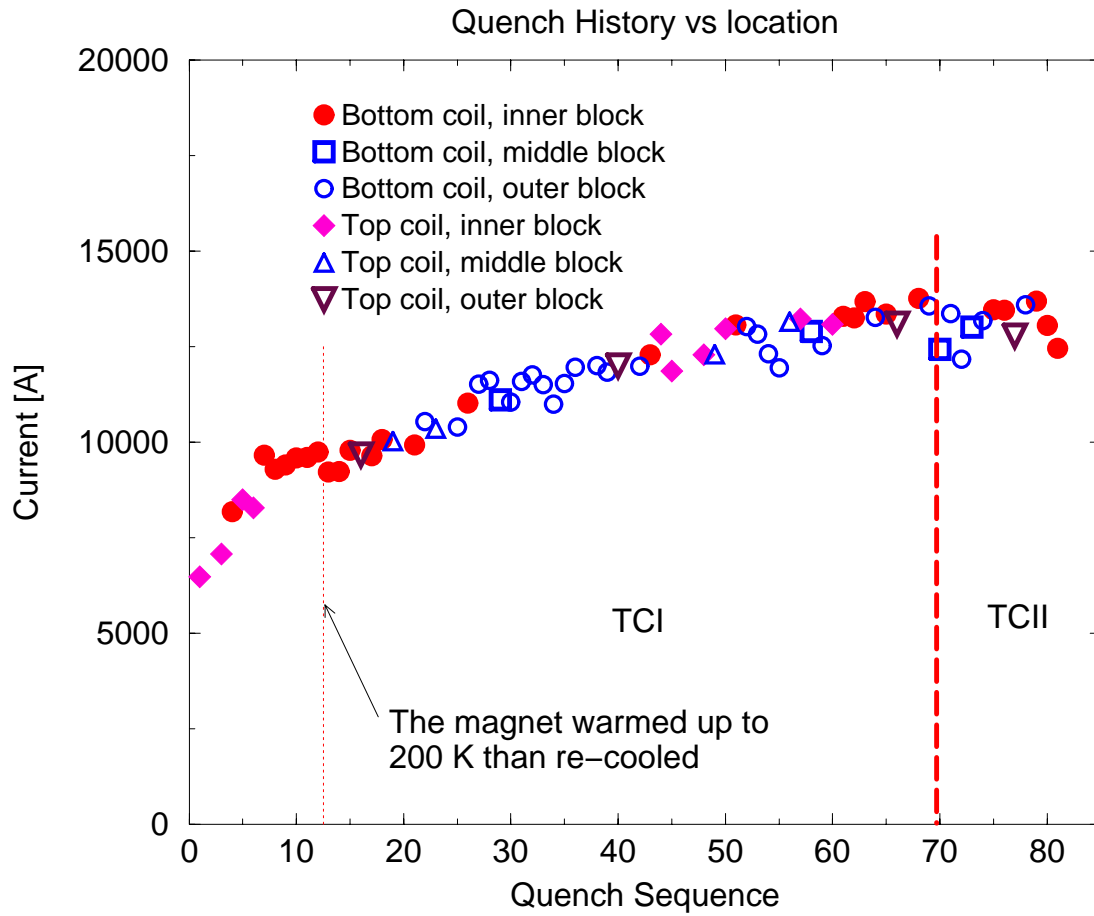


Figure 2. Quench history of HFDC01 as function of coil blocks.

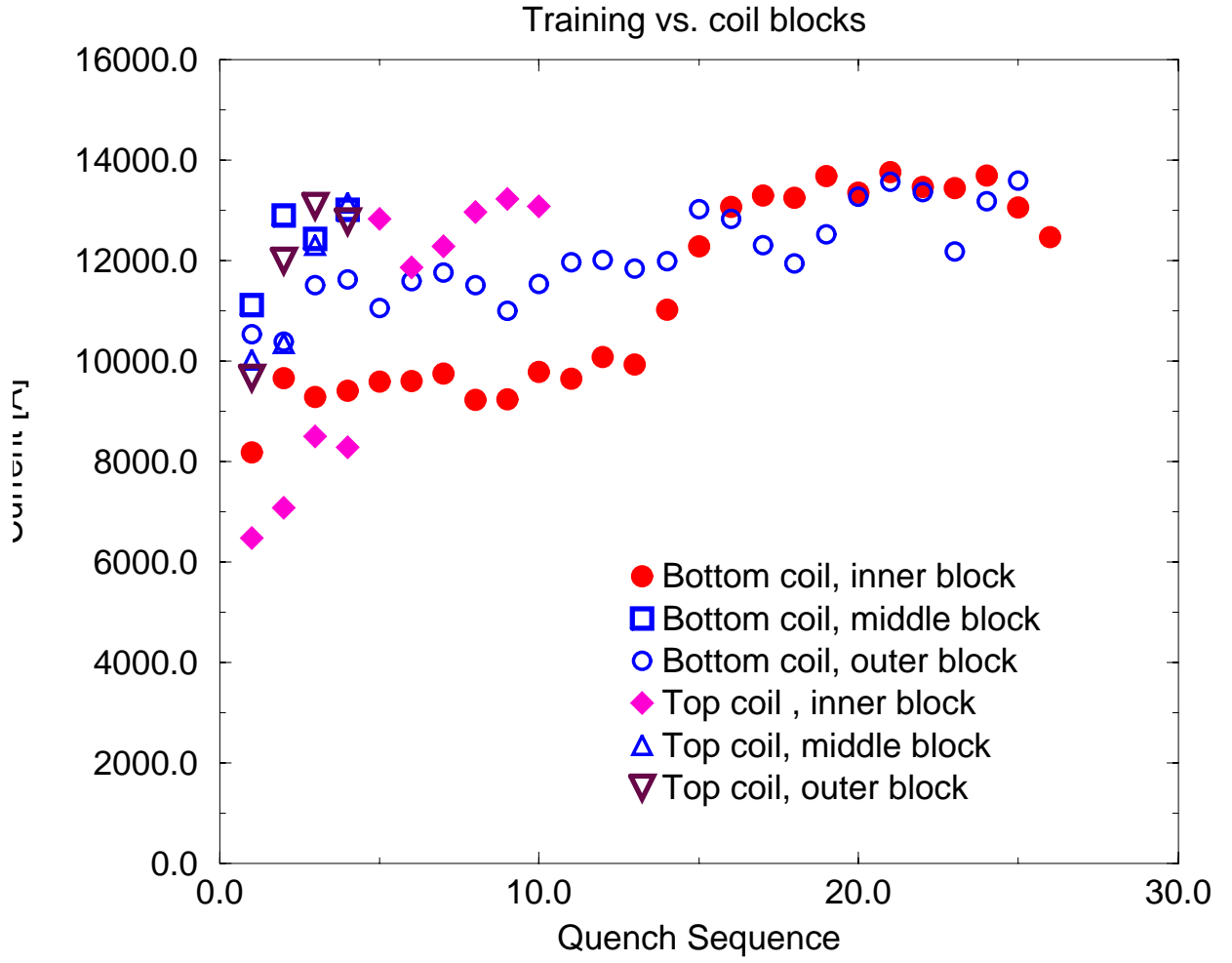


Figure 3. Quench training of HFDC01 as function of coil blocks.

### hfdc01.Quench.030916151234.485

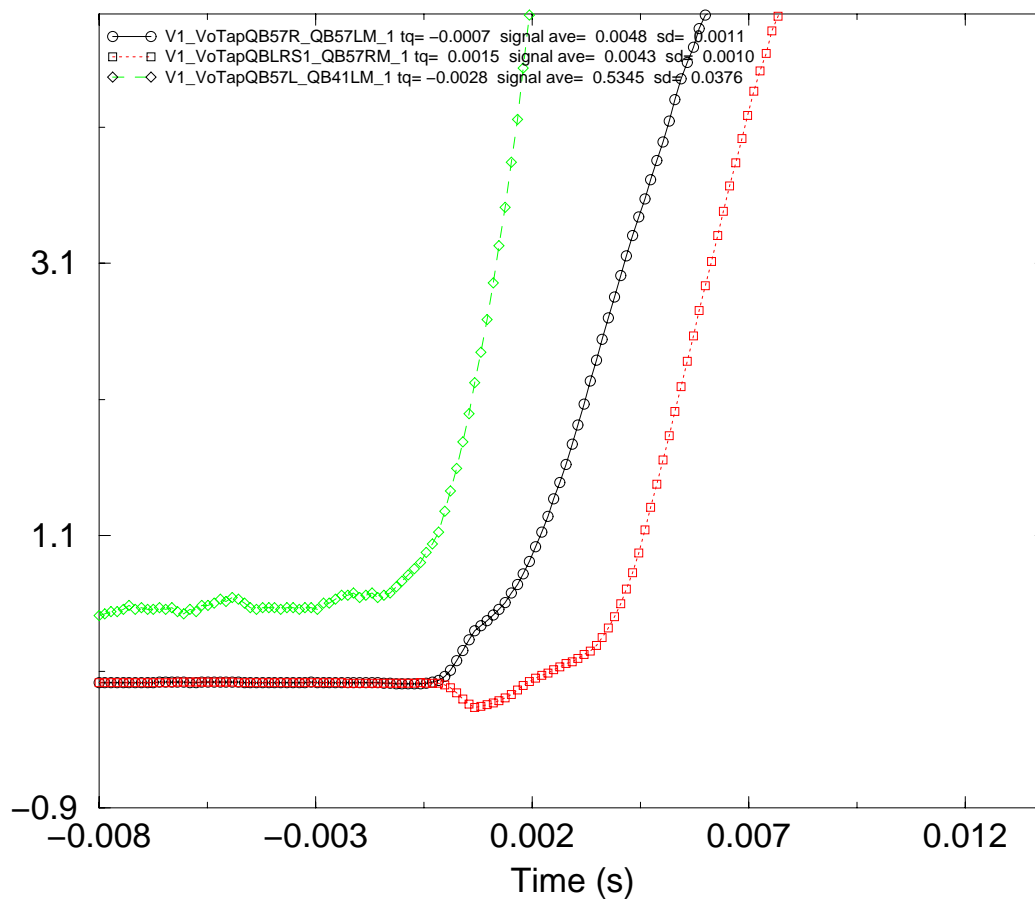


Figure 4. Typical quench (quench # 23).

hfdc01.Quench.030915195027.144

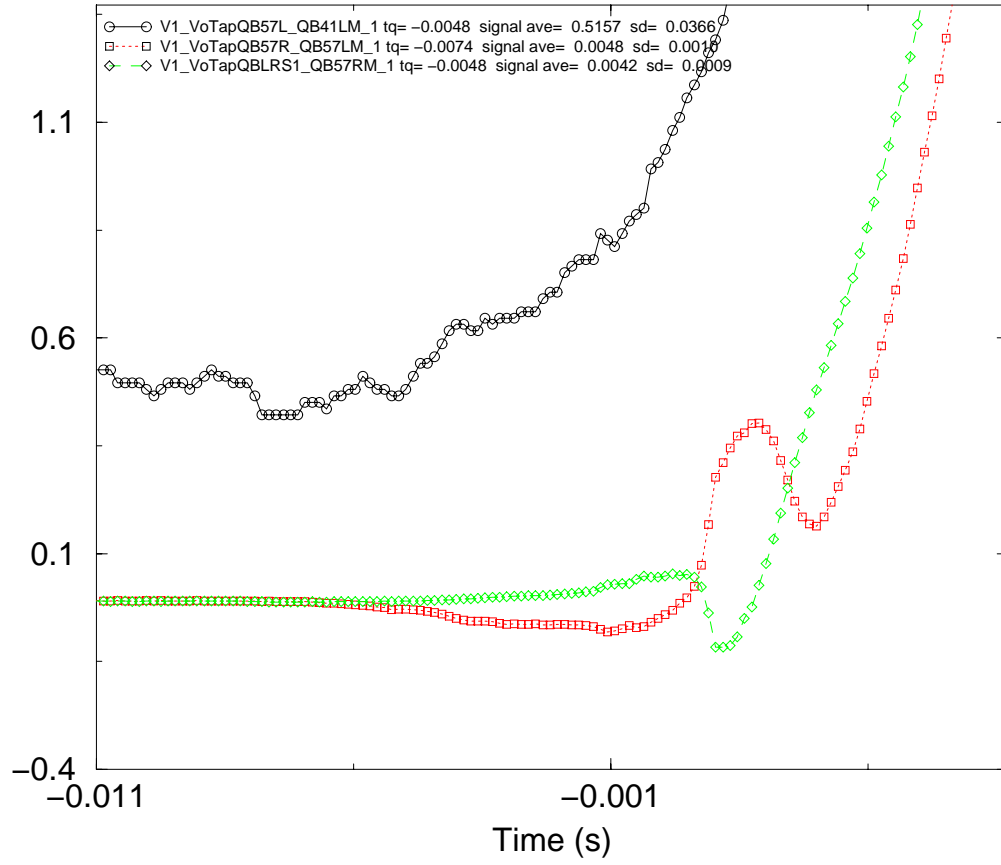


Figure 5. Quench #14 of HFDC01.

Table I

| File                                  | Quench No. | Current (Amps) | Nominal Ramp Rate | $t_{\text{quench}}$ | MIITs | QDC Trigger | Quench Vtap Seg #1 | Mag Bot Temp | File Comments                                    |
|---------------------------------------|------------|----------------|-------------------|---------------------|-------|-------------|--------------------|--------------|--|
| hfdc01.Quench.030808100654.376        |            | 13.8           | 0                 | 1.0000              | 0.00  | GndRef      | QB17L_QBHRS        | 88.464       | 0 amp trip to check how the file looks like      |
| <i>hfdc01.Quench.030808113111.668</i> |            |                |                   |                     |       |             |                    |              | <i>data file corrupted</i>                       |
| hfdc01.Quench.030808172606.067        |            | 12.8           | 0                 | -0.0361             | 0.04  | WcoilGnd    | QB17L_QBHRS        | 4.336        | trip during ramp up                              |
| hfdc01.Quench.030808173629.307        |            | 194.5          | 51                | 0.0004              | 0.04  | GndRef      | QB17R_QB17L        | 4.334        | another trip at 168A during a ramp               |
| hfdc01.Quench.030808175552.945        |            | 444.0          | -34               | -0.1666             | 0.09  | SIWcoil     | QB18L2_QB18L1      | 4.336        | trip due PS time constant change                 |
| hfdc01.Quench.030808184513.432        |            | 465.1          | 0                 | -0.3626             | 0.13  | WcoilGnd    | QB17R_QB17L        | 4.333        | trip during balancing                            |
| hfdc01.Quench.030808190013.190        |            | 2022.9         | 0                 | 0.0003              | 0.33  | GndRef      | QB17R_QB17L        | 4.329        | 2000A manual trip to check signals               |
| <i>hfdc01.Quench.030808192149.470</i> |            |                |                   |                     |       |             |                    |              | <i>data file corrupted</i>                       |
| hfdc01.Quench.030808195416.577        | <b>1</b>   | 6514.4         | 20                | -0.0207             | 3.63  | HcoilHcoil  | QTHRS_QT17L        | 4.318        | 6400A trip could be the first quench             |
| <i>hfdc01.Quench.030808202035.182</i> | <b>2</b>   |                |                   |                     |       |             |                    |              | <i>data file corrupted</i>                       |
| hfdc01.Quench.030808204356.640        | <b>3</b>   | 7113.5         | 20                | -0.0069             | 3.48  | HcoilHcoil  | QTHRS_QT17L        | 4.311        | 3 <sup>rd</sup> quench at 7078A, 20 A/sec        |
| hfdc01.Quench.030808210832.919        | <b>4</b>   | 8219.0         | 20                | -0.0045             | 3.94  | HcoilHcoil  | QB17L_QBHRS        | 4.306        | 8181A 4 <sup>th</sup> quench, 20A/sec            |
| hfdc01.Quench.030808213004.857        | <b>5</b>   | 8541.0         | 20                | -0.0046             | 4.14  | HcoilHcoil  | QTHRS_QT17L        | 4.306        | 5 <sup>th</sup> quench 8499A, 20a/sec            |
| hfdc01.Quench.030808214644.126        | <b>6</b>   | 8328.1         | 20                | -0.0056             | 4.02  | HcoilHcoil  | QTHRS_QT17L        | 4.301        | 6 <sup>th</sup> quench, 20a/sec, Iq=8287A        |
| hfdc01.Quench.030808221025.842        | <b>7</b>   | 9703.3         | 20                | -0.0031             | 3.97  | HcoilHcoil  | QB17R_QB17L        | 4.284        | 7 <sup>th</sup> Quench, 20A/sec, Iq=9658A        |
| hfdc01.Quench.030808223336.463        | <b>8</b>   | 9326.2         | 20                | -0.0024             | 3.72  | HcoilHcoil  | QB17L_QBHRS        | 4.279        | 8 <sup>th</sup> quench, 20a/sec, 9283A           |
| hfdc01.Quench.030808224845.064        | <b>9</b>   | 9445.5         | 301               | -0.0063             | 4.89  | HcoilHcoil  | QBLRS1_QB57R       | 4.283        | Iq=9404A, 300A/sec, 9 <sup>th</sup> quench       |
| hfdc01.Quench.030808231120.273        | <b>10</b>  | 9633.6         | 20                | -0.0050             | 4.17  | HcoilHcoil  | QB17L_QBHRS        | 4.276        | 10 <sup>th</sup> quench, 20a/sec, Iq=9590A       |
| hfdc01.Quench.030808233051.250        | <b>11</b>  | 9643.7         | 20                | -0.0028             | 4.48  | HcoilHcoil  | QBHRS_QBCHRS       | 4.280        | 11 <sup>th</sup> quench, Iq=9600A, 20A/sec       |
| hfdc01.Quench.030808234856.391        | <b>12</b>  | 9795.0         | 20                | -0.0034             | 3.76  | HcoilHcoil  | QB17R_QB17L        | 4.306        | 12 <sup>th</sup> quench, Iq=9750a, 20a/sec       |
| hfdc01.Quench.030915173106.750        |            | 378.9          | 350               | -0.0001             | 0.05  | HcoilHcoil  | QB40L_QB39R        | 4.377        | trip during balancing                            |
| hfdc01.Quench.030915174604.029        |            | 2016.4         | 0                 | 0.0018              | 0.32  | WcoilGnd    | QB39L1_QB18L2      | 4.373        | 2000A maual trip                                 |
| hfdc01.Quench.030915184850.587        |            | 5034.7         | 0                 | -0.1022             | 3.71  | HcoilHcoil  | QTHRS_QT17L        | 4.374        | 5000A, SHFU=300V, 4.3K                           |
| hfdc01.Quench.030915191515.475        | <b>13</b>  | 9266.6         | 20                | -0.0052             | 3.70  | HcoilHcoil  | QB17R_QB17L        | 4.377        | 13 <sup>th</sup> quench, Iq=9224A, 20A/sec, 4.3K |
| hfdc01.Quench.030915195027.144        | <b>14</b>  | 9281.3         | 20                | -0.0045             | 4.39  | HcoilHcoil  | QB57R_QB57L        | 4.375        | 14 <sup>th</sup> quench, Iq=9238A, 20A/sec, 4.3K |
| hfdc01.Quench.030915212925.748        | <b>15</b>  | 9836.3         | 20                | -0.0046             | 4.21  | WcoilIdot   | QB17L_QBHRS        | 4.384        | 15 <sup>th</sup> quench, Iq=9788A, 20A/sec, 4.3K |

|                                       |           |         |    |         |      |            |               |       |  |
|---------------------------------------|-----------|---------|----|---------|------|------------|---------------|-------|--|
| hfdc01.Quench.030915220014.690        | 16        | 9715.2  | 20 | -0.0004 | 4.11 | WcoilIdot  | QT40L_QT41L   | 4.380 | 16 <sup>th</sup> quench, Iq=9672A, 20a/sec, 4.3K   |
| hfdc01.Quench.030915222954.036        | 17        | 9694.1  | 20 | -0.0056 | 4.26 | HcoilHcoil | QB17L_QBHRS   | 4.380 | 17 <sup>th</sup> quench, Iq=9649A, 20A/sec, 4.3K   |
| hfdc01.Quench.030915225032.838        | 18        | 10123.5 | 20 | -0.0034 | 4.31 | HcoilHcoil | QB17L_QBHRS   | 4.391 | 18 <sup>th</sup> quench, Iq=10078A, 20a/sec, 4.3K  |
| hfdc01.Quench.030915231313.029        | 19        | 10071.2 | 20 | -0.0038 | 3.99 | HcoilHcoil | QT39R_QT40L   | 4.388 | 19 <sup>th</sup> quench, Iq=10027A, 20A/sec, 4.3K  |
| <b>hfdc01.Quench.030916084604.001</b> | <b>20</b> |         |    |         |      |            |               |       | <b>data file corrupted</b>                         |
| hfdc01.Quench.030916091211.508        | 21        | 9977.6  | 20 | -0.0039 | 3.97 | HcoilHcoil | QB17L_QBHRS   | 4.412 | 21 <sup>st</sup> quench, Iq=100000A, 20A/sec, 4.3K |
| hfdc01.Quench.030916093518.516        | 22        | 10584.0 | 20 | -0.0032 | 4.49 | HcoilHcoil | QB57R_QB57L   | 4.425 | 22 <sup>nd</sup> quench, Iq=10536A, 20A/sec, 4.3K  |
| hfdc01.Quench.030916100240.895        | 23        | 10397.8 | 20 | -0.0045 | 4.64 | HcoilHcoil | QT18L2_QT39L1 | 4.432 | 23 <sup>rd</sup> quench, Iq=10351A, 20A/sec, 4.3K  |
| <b>hfdc01.Quench.030916102416.006</b> | <b>24</b> |         |    |         |      |            |               |       | <b>data file corrupted</b>                         |
| hfdc01.Quench.030916104950.755        | 25        | 10438.1 | 20 | -0.0106 | 5.13 | HcoilHcoil | QB57R_QB57L   | 4.479 | 26 <sup>th</sup> quench, Iq=10391A, 20A/sec, 3.4K  |
| hfdc01.Quench.030916111732.024        | 26        | 11072.1 | 20 | -0.0006 | 4.32 | WcoilIdot  | QB17L_QBHRS   | 4.603 | 26 <sup>th</sup> quench, Iq=11024A, 20A/sec, 4.3K  |
| hfdc01.Quench.030916114718.872        | 27        | 11563.8 | 20 | -0.0024 | 3.99 | HcoilHcoil | QB41L_QB40L   | 4.495 | 27 <sup>th</sup> quench, Iq=11515A, 20A/sec, 4.3K  |
| hfdc01.Quench.030916122843.949        | 28        | 11678.5 | 20 | -0.0018 | 4.13 | WcoilIdot  | QB57L_QB41L   | 4.518 | 28 <sup>th</sup> quench, Iq=11626A, 20A/sec, 4.3KP |
| hfdc01.Quench.030916130339.980        | 29        | 11159.2 | 20 | -0.0073 | 4.49 | WcoilIdot  | QB40L_QB39R   | 4.507 | 29 <sup>th</sup> quench, Iq=11113A, 20A/sec, 4.3K  |
| hfdc01.Quench.030916143128.396        | 30        | 11106.0 | 20 | -0.0034 | 4.12 | HcoilHcoil | QB57R_QB57L   | 4.465 | Quench #30 @4.4K, 20Amps/sec,                      |
| hfdc01.Quench.030916151234.485        | 31        | 11642.7 | 20 | -0.0018 | 4.43 | HcoilHcoil | QBLRS1_QB57R  | 4.467 | 31 <sup>st</sup> quench, Iq=11591A, 20A/sec, 4.3K  |
| hfdc01.Quench.030916155418.704        | 32        | 11815.1 | 20 | -0.0035 | 4.93 | HcoilHcoil | QB57L_QB41L   | 4.468 | 32 <sup>th</sup> quench, Iq=11763A, 20A/sec, 4.3K  |
| hfdc01.Quench.030916162816.253        | 33        | 11561.9 | 20 | -0.0015 | 3.74 | HcoilHcoil | QB57R_QB57L   | 4.469 | 33 <sup>rd</sup> quench, Iq=11511A, 20A/sec, 4.3K  |
| hfdc01.Quench.030916170935.612        | 34        | 11044.5 | 20 | -0.0032 | 4.57 | HcoilHcoil | QB57R_QB57L   | 4.463 | 34 <sup>th</sup> quench, Iq=10996A, 20A/sec, 4.3K  |
| hfdc01.Quench.030916174020.615        | 35        | 11582.1 | 20 | -0.0021 | 4.56 | WcoilIdot  | QBLRS1_QB57R  | 4.461 | 35 <sup>th</sup> quench, Iq=11531A, 20A/sec, 4.3K  |
| hfdc01.Quench.030916182043.561        | 36        | 12017.9 | 20 | -0.0042 | 4.30 | SIWcoil    | QB57R_QB57L   | 4.454 | 36 <sup>th</sup> quench, Iq=11966A, 20A/sec, 4.3K  |
| <b>hfdc01.Quench.030916190513.256</b> | <b>37</b> |         |    |         |      |            |               |       | <b>data file corrupted</b>                         |
| hfdc01.Quench.030916195454.870        | 38        | 12059.2 | 20 | -0.0021 | 4.14 | HcoilHcoil | QB57R_QB57L   | 4.443 | 38 <sup>th</sup> quench, Iq=12007A, 20A/sec, 4.3K  |
| hfdc01.Quench.030916203405.796        | 39        | 11889.5 | 20 | -0.0038 | 4.20 | HcoilHcoil | QB57R_QB57L   | 4.444 | 39 <sup>th</sup> quench, Iq=11837, 20A/sec, 4.3K   |
| hfdc01.Quench.030916210936.220        | 40        | 12055.5 | 20 | -0.0049 | 4.14 | HcoilHcoil | QT40L_QT41L   | 4.452 | 40 <sup>th</sup> quench, Iq=12003A, 20A/sec, 4.3K  |
| <b>hfdc01.Quench.030917113550.755</b> | <b>41</b> |         |    |         |      |            |               |       | <b>data file corrupted</b>                         |
| hfdc01.Quench.030917125932.176        | 42        | 12039.9 | 20 | -0.0116 | 6.19 | GndRef     | QB57R_QB57L   | 2.154 | 42 <sup>nd</sup> quench, Iq=12000A, 20A/sec, 2.2K  |
| hfdc01.Quench.030917140552.044        | 43        | 12342.6 | 20 | -0.0028 | 4.87 | HcoilHcoil | QB17L_QBHRS   | 2.350 | 43 <sup>rd</sup> quench, Iq=12287A, 20A/sec, 2.5K  |
| hfdc01.Quench.030917143922.585        | 44        | 12883.0 | 20 | -0.0013 | 4.72 | HcoilHcoil | QTHRS_QT17L   | 2.853 | 33 <sup>th</sup> quench, Iq=12827A, 20A/sec, 4.2K  |
| hfdc01.Quench.030917152303.006        | 45        | 11920.6 | 20 | -0.0014 | 4.66 | HcoilHcoil | QTHRS_QT17L   | 4.447 | 45 <sup>th</sup> quench, Iq=11868A, 20a/sec, 4.3K  |
| <b>hfdc01.Quench.030917155345.714</b> | <b>46</b> |         |    |         |      |            |               |       | <b>data file corrupted</b>                         |

|                                       |           |         |    |         |      |            |               |       |   |
|---------------------------------------|-----------|---------|----|---------|------|------------|---------------|-------|---|
| <i>hfdc01.Quench.030917162552.079</i> | <b>47</b> |         |    |         |      |            |               |       | <i>data file corrupted</i>  |
| hfdc01.Quench.030917165858.830        | <b>48</b> | 12339.9 | 20 | -0.0020 | 4.92 | HcoilHcoil | QTHRS_QT17L   | 4.454 | 48 <sup>th</sup> quench, Iq=12286A, 20A/sec, 4.3K   |
| hfdc01.Quench.030917173750.154        | <b>49</b> | 12361.9 | 20 | -0.0042 | 4.36 | HcoilHcoil | QT18L1_QT18L2 | 4.469 | 49 <sup>th</sup> quench, Ic=12308A, 20a/sec, 4.3K   |
| hfdc01.Quench.030917181301.582        | <b>50</b> | 13027.9 | 20 | -0.0014 | 4.62 | HcoilHcoil | QTHRS_QT17L   | 4.477 | 50 <sup>th</sup> quench, Iq=12969A, 20a/sec, 4.3K   |
| hfdc01.Quench.030917185337.705        | <b>51</b> | 13130.7 | 20 | -0.0018 | 5.01 | HcoilHcoil | QB17L_QBHRS   | 4.486 | 51 <sup>st</sup> quench, Iq=13072A, 20A/sec, 4.3K   |
| hfdc01.Quench.030917193501.669        | <b>52</b> | 13083.9 | 20 | -0.0013 | 3.92 | HcoilHcoil | QB57R_QB57L   | 4.499 | Quench at I= 13029 A, Ramp arte = 20 A/s  |
| hfdc01.Quench.030917202211.674        | <b>53</b> | 12888.5 | 20 | -0.0020 | 4.14 | WcoilIdot  | QB57R_QB57L   | 4.427 | 53rg quench, Iq=12830A, 20a/sec, 4.3K   |
| hfdc01.Quench.030917205651.292        | <b>54</b> | 12363.7 | 20 | -0.0021 | 3.99 | HcoilHcoil | QB57R_QB57L   | 4.477 | 54 <sup>th</sup> quench, Iq=12311A, 20a/sec, 4.3K0  |
| hfdc01.Quench.030917212952.735        | <b>55</b> | 11995.0 | 20 | -0.0048 | 4.33 | HcoilHcoil | QBLRS1_QB57R  | 4.492 | 55 <sup>th</sup> quench, Iq=11942A, 20A/sec, 4.3K   |
| hfdc01.Quench.030918120640.571        |           | 14.7    | 0  | 1.0000  | 0.00 | GndRef     | QB17L_QBHRS   | 4.019 | trigger by hand to test analytek data capture   |
| hfdc01.Quench.030918122326.202        |           | 15.6    | 0  | 1.0000  | 0.00 | GndRef     | QB17L_QBHRS   | 4.036 | another manual trip at zero Amps, no heaters. Checking signals on analytek data logger looking at 4 strain gauge bullets. This time chain has 0.1 mA current through str. Gauges  |
| hfdc01.Quench.030918133958.444        |           | 17.4    | 0  | 1.0000  | 0.00 | GndRef     | QB17L_QBHRS   | 4.103 | another test of fast strain gauge readout with analytek. SG current = 0.5mA. MUX cables from Switchboxes 1 and 2 were disconnected from switchbox, to see if this changes the noise and/or voltage levels seen  |
| hfdc01.Quench.030918140134.398        |           | 19.3    | 0  | 1.0000  | 0.00 | GndRef     | QB17L_QBHRS   | 4.128 | another test of fast analytek data capture. I changed polarities of all the strain gauge inputs   |
| hfdc01.Quench.030918141826.422        |           | 3732.0  | 22 | -0.0025 | 1.05 | HcoilHcoil | QB39L1_QB18L2 | 4.148 | triggered on a "snapshot" pulse = DQD_Coil triggered on half coil difference threshold of 0.1 Volt. This is to capture the full quench characterization data set (including quench antenna) for one or more "snapshot" glitches. (Normal half coil threshold is .5V) Note that we are also instrumenting 4 strain gauge channels with analytek data logger during the quench.Coef |
| hfdc01.Quench.030918144006.417        |           | 3214.6  | 20 | -0.0031 | 0.79 | HcoilHcoil | QT57L_QT57R   | 4.177 | another snapshot trigger at 0.1V on DQD half coil with full data acquisition.f  |
| hfdc01.Quench.030918145110.235        |           | 3410.9  | 20 | -0.0015 | 0.87 | HcoilHcoil | QT39R_QT40L   | 4.199 | 3 <sup>rd</sup> "snapshot" data capture event to look at full data acquisition triggered on 100mV half coil glitch.   |
| Hfcdc01.Quench.030918150044.554       |           | 3546.7  | 0  | -0.5077 | 7.33 | HcoilHcoil | QB57L_QB41L   | 4.211 | 4 <sup>th</sup> snapshot trigger at .1V   |
| hfdc01.Quench.030918151148.848        |           | 3099.9  | 20 | -0.0926 | 1.60 | HcoilHcoil | QT57L_QT57R   | 4.227 | 5 <sup>th</sup> snapshot data sety  |
| hfdc01.Quench.030918154423.552        | <b>56</b> | 13208.7 | 19 | -0.0036 | 4.67 | WcoilIdot  | QT39L2_QT39R  | 4.277 | ramp to quench at 20A/s. 4.5K. We captured fast strain gauge bullet data (4 bullets) with analytek. Heaters delayed by 10ms, dump delay by 25ms.  |
| Hfcdc01.Quench.030919172129.003       | <b>57</b> | 13283.0 | 20 | -0.0017 | 4.50 | HcoilHcoil | QT17L_QT18L1  | 4.392 | Ramp to quench  |

|                                       |           |         |      |         |       |            |               |       |  |
|---------------------------------------|-----------|---------|------|---------|-------|------------|---------------|-------|--|
| hfdc01.Quench.030919194412.952        | <b>58</b> | 12954.5 | 20   | -0.0057 | 4.93  | HcoilHcoil | QB39L2_QB39L1 | 4.402 | Cleansing quench   |
| hfdc01.Quench.030920102700.047        | <b>59</b> | 12579.3 | 20   | -0.0014 | 4.00  | HcoilHcoil | QB57R_QB57L   | 4.398 | Cleansing Quench   |
| hfdc01.Quench.030920113335.393        | <b>60</b> | 13140.8 | 19   | -0.0015 | 4.96  | HcoilHcoil | QTHRS_QT17L   | 4.395 | Cleansing quench   |
| hfdc01.Quench.030920145729.995        | <b>61</b> | 13362.8 | 1    | -0.1228 | 26.47 | WcoilGnd   | QBHRS_QBCHRS  | 4.388 | Current 12500A at20A/s ramp rate, then 2A/s up to the quench at 13293A |
| hfdc01.Quench.030920155705.747        | <b>62</b> | 13305.9 | 1    | -0.0013 | 4.74  | HcoilHcoil | QBHRS_QBCHRS  | 4.392 | Cleansing quench   |
| hfdc01.Quench.030920193111.990        | <b>63</b> | 13740.8 | 20   | -0.0014 | 4.90  | HcoilHcoil | QBHRS_QBCHRS  | 4.383 | Cleansing quench at 13681A   |
| hfdc01.Quench.030922112841.745        | <b>64</b> | 13323.3 | 20   | -0.0017 | 4.01  | SIWcoil    | QB57R_QB57L   | 4.452 | Cleansing quench   |
| hfdc01.Quench.030922134514.421        | <b>65</b> | 13416.0 | 20   | -0.0060 | 5.63  | HcoilHcoil | QBHRS_QBCHRS  | 4.512 | Cleansing quench   |
| hfdc01.Quench.030922150822.413        | <b>66</b> | 13127.0 | 20   | -0.0013 | 4.00  | HcoilHcoil | QT57R_QTLRS1  | 4.530 | Cleansing quench   |
| <b>hfdc01.Quench.030922164755.419</b> | <b>67</b> |         |      |         |       |            |               |       | <b>data file corrupted</b>   |
| hfdc01.Quench.030922185539.768        | <b>68</b> | 13825.2 | 20   | -0.0007 | 4.80  | HcoilHcoil | QB17L_QBHRS   | 4.514 | Cleansing quench   |
| hfdc01.Quench.030922205554.735        | <b>69</b> | 13627.0 | 20   | -0.0007 | 3.92  | HcoilHcoil | QBLRS1_QB57R  | 4.493 | Cleansing Quench   |
| hfdc01.Quench.031016134700.518        |           | 1009.1  | 0    | 0.0031  | 0.11  | WcoilIdot  | QB40L_QB39R   | 4.458 | 1000A manual trip  |
| hfdc01.Quench.031016143028.501        |           | 1011.0  | 0    | -0.0305 | 0.14  | WcoilGnd   | QB41L_QB40L   | 4.452 | another 1000A manual trip  |
| hfdc01.Quench.031016144511.757        |           | 1008.2  | 0    | 0.0024  | 0.11  | WcoilGnd   | QB39L1_QB18L2 | 4.453 | 1000A manual tripef  |
| hfdc01.Quench.031016151017.228        |           | 1008.2  | 0    | 0.0029  | 0.11  | WcoilGnd   | QB57R_QB57L   | 4.454 | 1000A trip   |
| hfdc01.Quench.031016152031.386        |           | 2454.0  | 19   | 0.0001  | 0.32  | WcoilIdot  | QB17L_QBHRS   | 4.456 | aqd lead trip  |
| hfdc01.Quench.031016161842.656        | <b>70</b> | 12481.2 | 21   | -0.0024 | 4.13  | HcoilHcoil | QB40L_QB39R   | 4.465 | 70 <sup>th</sup> quench, Iq=12431A, 20A/sec, 4.5K                      |
| hfdc01.Quench.031016172511.455        | <b>71</b> | 13424.3 | 0    | -0.0017 | 4.55  | HcoilHcoil | QBLRS1_QB57R  | 4.467 | 71 <sup>st</sup> quench, Iq=13367A, 20A/sec, 4.5K                      |
| hfdc01.Quench.031016180013.158        | <b>72</b> | 12232.6 | 20   | -0.0042 | 4.37  | HcoilHcoil | QBLRS1_QB57R  | 4.477 | Iq = 12179 ramp = 20 A/s quench # 72                                   |
| hfdc01.Quench.031016182700.655        | <b>73</b> | 13061.0 | 20   | -0.0014 | 4.85  | HcoilHcoil | QB39L1_QB18L2 | 4.484 | Iq=13008 rate 20A/sec quench number 73                                 |
| hfdc01.Quench.031016185823.998        | <b>74</b> | 13240.8 | 20   | -0.0024 | 4.27  | HcoilHcoil | QB39L2_QB39L1 | 4.473 | Iq=13183 rate 20A/sec Quench num 74                                    |
| hfdc01.Quench.031016203343.370        | <b>75</b> | 13528.8 | 20   | -0.0010 | 4.72  | HcoilHcoil | QBHRS_QBCHRS  | 4.452 | Iq = 13470 A, ramp = 20 A/s Quench # 75                                |
| hfdc01.Quench.031016212033.547        | <b>76</b> | 13505.9 | 20   | -0.0010 | 4.80  | HcoilHcoil | QB17L_QBHRS   | 4.469 | 76 <sup>th</sup> quench, Iq=13446A, 20A/sec, 4.5K                      |
| hfdc01.Quench.031017132145.768        | <b>77</b> | 12845.4 | 19   | -0.0010 | 5.29  | HcoilHcoil | QT57R_QTLRS1  | 4.503 | Cleansing quench   |
| hfdc01.Quench.031017165919.760        |           | 2229.3  | -150 | -0.0139 | 0.47  | WcoilIdot  | QB17R_QB17L   | 4.495 | system tripped or quench while ramping down from 6500 amps             |
| hfdc01.Quench.031017173003.893        |           | 1978.8  | -150 | -0.0641 | 0.57  | HcoilHcoil | QT17L_QT18L1  | 4.494 | Quench while ramping down -- eieo                                      |
| hfdc01.Quench.031020114802.289        |           | 10038.1 | 0    | -0.0042 | 3.61  | WcoilIdot  | QB18L1_QB17R  | 4.471 | quench at 10 kA, spot heater TSH18                                     |
| hfdc01.Quench.031020124914.391        |           | 10038.1 | 0    | -0.0043 | 3.71  | HcoilHcoil | QB18L1_QB17R  | 4.490 | Temp induced quench at 10 kA, t=7.8 K BSH18                            |
| hfdc01.Quench.031020134617.398        |           | 12045.4 | 0    | -0.0046 | 4.36  | SIWcoil    | QB18L1_QB17R  | 4.499 | Temperature induced quench I=12kA, t=7.7K BSH18                        |
| hfdc01.Quench.031020143132.914        |           | 9900.5  | 40   | -0.0032 | 3.76  | HcoilHcoil | QB18L1_QB17R  | 4.498 | Quench at about 10 kA with temp at BSH18 8.5 K                         |
| hfdc01.Quench.031020151007.641        |           | 11336.3 | 4    | -0.0020 | 4.09  | HcoilHcoil | QB18L1_QB17R  | 4.500 | Iq=11304 A ramp=5A/s, t=8K BSH18                                       |
| hfdc01.Quench.031020155936.669        |           | 13316.9 | 4    | -0.0069 | 5.24  | HcoilHcoil | QB18L2_QB18L1 | 4.503 | Quench # 6 (SH series) Iq=13280, ramp=5A/s T=7.9 TSH18                 |

|                                |           |         |       |         |      |            |               |         |   |
|--------------------------------|-----------|---------|-------|---------|------|------------|---------------|---------|---|
| hfdc01.Quench.031020163422.761 |           | 1550.4  | 0     | -0.3981 | 1.17 | HcoilHcoil | QT18L1_QT18L2 | 4.531   | Quench #7 of spot heater series Iq= 1500 A at 20 A/s  |
| hfdc01.Quench.031020170033.960 |           | 10040.9 | 0     | -0.0048 | 3.88 | WcoilGnd   | QT18L1_QT18L2 | 4.495   | Quench #8 of Spot Heater series Iq=10kA, Temp=8.1K  |
| hfdc01.Quench.031020172029.121 |           | 2752.2  | 20    | -0.1008 | 1.31 | HcoilHcoil | QT18L1_QT18L2 | 4.515   | Quench #9 of SH series Iq=2745 A, ramp=20 A/s<br>Temp=9K at TSH18                                     |
| hfdc01.Quench.031020181313.889 |           | 13455.4 | 5     | -0.0034 | 5.02 | HcoilHcoil | QT39R_QT40L   | 4.482   | Quench #10 of spot heater series, Iq=13416 A, ramp<br>=5A/s Temp=8K at TSH18                          |
| hfdc01.Quench.031020191610.241 |           | 13048.1 | 0     | -0.0015 | 4.12 | HcoilHcoil | QT18L1_QT18L2 | 4.487   | Quench # 11 Spot Heater series, Iq=13kA Temp = 7.9 K<br>at TSH18                                      |
| hfdc01.Quench.031020200240.470 |           | 7030.9  | 0     | -0.0090 | 2.78 | HcoilHcoil | QT18L1_QT18L2 | 4.492   | Quench # 12 SH series, Iq=7000A Temp=8.5K TSH18   |
| hfdc01.Quench.031020211747.072 |           | 13048.1 | 0     | -0.0021 | 3.99 | HcoilHcoil | QB39L2_QB39L1 | 4.474   | Quench #13 SH series - temp = 9.25K BSH39   |
| hfdc01.Quench.031021141315.689 |           | 3791.6  | 10    | -0.0371 | 1.54 | HcoilHcoil | QB18L1_QB17R  | 4.490   | Quench #14 of SH series Iq=3750A ramp =10 A/s<br>T=9.1K BSH18   |
| hfdc01.Quench.031021144211.037 |           | 10051.9 | 0     | -0.0034 | 3.63 | HcoilHcoil | QB18L2_QB18L1 | 4.498   | Quench #15 of SH series at 10kA while increasing<br>temperature to 8K TSH18                           |
| hfdc01.Quench.031021165819.929 |           | 6798.8  | 49837 | -0.0063 | 2.73 | HcoilHcoil | QB18L1_QB17R  | 4.503   | Quench #16 of SH series Iq=6765A ramp=5 A/s<br>temp=8.5K  |
| hfdc01.Quench.031021172807.998 |           | 10053.7 | 0     | -0.0031 | 3.58 | HcoilHcoil | QB18L1_QB17R  | 4.511   | Quench #17 of SH series Iq=10000 T=8.05K TSH18  |
| hfdc01.Quench.031021185948.672 |           | 13066.5 | 0     | -0.0017 | 4.07 | HcoilHcoil | QB18L2_QB18L1 | 4.523   | Quench #18 at Iq=13 kA Temp=7.68K TSH18   |
| hfdc01.Quench.031021203208.332 |           | 11561.0 | 0     | -0.0027 | 3.95 | HcoilHcoil | QB18L1_QB17R  | 4.516   | Quench #19 SH series Iq=11500A T=7.85K BSH18  |
| hfdc01.Quench.031021213604.485 |           | 13068.3 | 0     | -0.0018 | 4.16 | HcoilHcoil | QT18L1_QT18L2 | 4.521   | Quench # 20 SH series Iq=13000 Temp=8K TSH18  |
| hfdc01.Quench.031022114252.735 | <b>78</b> | 13649.0 | 21    | -0.0048 | 4.83 | WcoilGnd   | QB57R_QB57L   | 4.492   | Quench num 78 rate 20 A/s Iq=13589  |
| hfdc01.Quench.031022122755.998 | <b>79</b> | 13755.4 | 21    | -0.0035 | 5.11 | HcoilHcoil | QBHRS_QBCHRS  | 4.532   | Quench num 79 rate 20A/sec Iq=13677   |
| hfdc01.Quench.031022132755.319 | <b>80</b> | 13111.4 | 301   | -0.0011 | 4.52 | HcoilHcoil | QBHRS_QBCHRS  | 4.509   | Quench #80 Iq=13054 A ramp=300 A/s  |
| hfdc01.Quench.031022140053.842 | <b>81</b> | 12518.8 | 151   | -0.0018 | 4.68 | HcoilHcoil | QBHRS_QBCHRS  | 4.560   | Quench #81 Iq=12462 A ramp= 150 A/s   |
| hfdc01.Quench.031022152259.455 |           | 12060.1 | 0     | -0.0031 | 4.00 | HcoilHcoil | QB39L2_QB39L1 | 4.493   | Quench #21 SH series at 120000 A Temp = 8.8 K<br>BSH39  |
| hfdc01.Quench.031030151512.786 |           | 3028.3  | 0     | 1.0000  | 0.00 | GndRef     | QBLqc_QBLRS2  | 290.727 | This is a test of analytek data saving – current is faked by<br>datel voltage source. This is test #1 |

### 3 Temperature margin measurements

Measurements of the local temperature margin have been performed during the third thermal cycle using the same procedure adopted for HFDB02 (describe in TD-02-024) and HFDA03A (TD-03-015). In the following we report briefly the procedure and the results.

Measurements were performed both at constant current and at constant temperature. In the first case the current in the coil was set at a constant value, below or equal to 13 kA. Subsequently the cable temperature was raised, by powering a 2.5 cm long spot heater (15 mm wide) with DC current. The temperature rise in the cable was measured by a calibrated Cernox sensor, glued to the cable, set a few mm distant from the spot heater edge. During the first measurements the heater current was raised in small steps, waiting for equilibrium conditions after each step (Fig. 6) until a quench occurred. In the following measurements the steps were significantly reduced in order to better simulate a slow linear temperature increase (Fig. 7).

During the measurement at fixed temperature, the temperature was raised at zero current (or at a current lower than the expected quench current). Subsequently after reaching a stable temperature the current was increased at fixed ramp rate until a quench occurred.

Measurements were performed using the spot heaters: BSH18, TSH18 and BSH39. The spot heater TSH39 couldn't be used because its circuit was open.

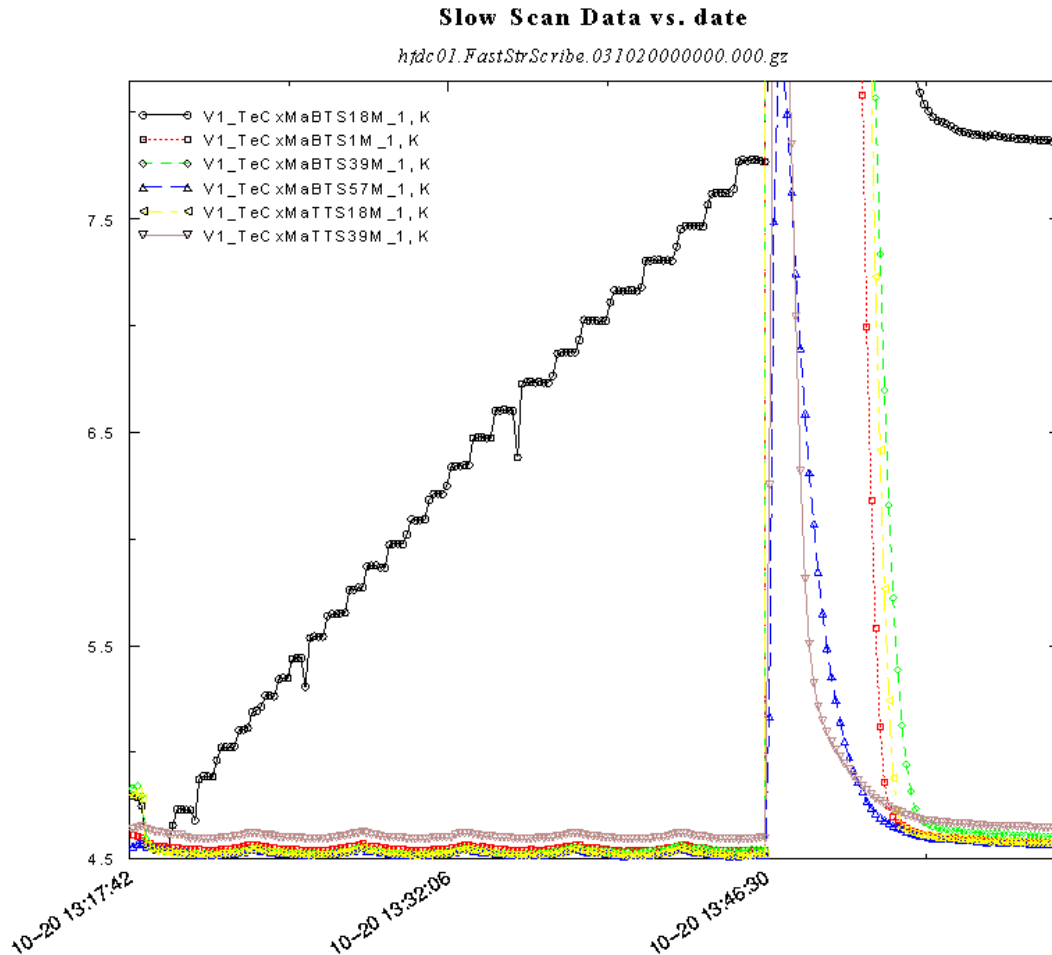
Figure 8 shows the values of temperature and current at which all quench occurred. It should be noted that the temperatures shown are the raw data without any correction. The maximum temperature under the spot heater should be higher than the temperature recorded at the sensor location. Finite-element models were developed in order to evaluate this difference in other magnets, but the scattering of the results obtained with this magnet made it impossible to do a similar correction. The open marks in Fig. 8 indicate measurements performed by increasing the current. All quenches started from the location of the spot heater being used, with the exception of two quenches indicated by red open marks (those should be regarded as erratic or training quenches typically occurring above 13 kA). The scattering of the results obtained with any spot heater is evident. It should also be noticed that the temperature scale in the plot has been significantly enlarged. In a full-scale plot all quenches fit in a small temperature range showing a temperature dependence very different from the dependence computed by using Nb3Sn parameterizations.

Figure 9 shows the results of all measurements performed using the spot heater BSH18. The ramp rates are shown for all measurements performed by increasing the current. The rate of the temperature increment (temperature/time step) is reported for some measurements performed by increasing the temperature. It can be noted that the "best results" (highest quench current over short sample limit at the same temperature, for instance  $I=13000\text{A}$   $T=7.68\text{K}$  in Fig.9) were obtained with the smallest temperature increments. Measurements performed using the other spot heaters showed similar behaviors.

Figure 10 shows a typical voltage rise in the segment under the spot heater and in an adjacent segment. When the quench started in the segment under the spot heater, a large

negative signal was recorded in the adjacent segment. The other adjacent segment had a large noise and it was not possible to do a similar analysis.

The expected quench current was computed for the “best result” obtained with BSH18 ( $I=13$  kA,  $T=7.68$  K). The short sample limit was computed by scaling the critical current of witness samples (heat treated with the coils) extracted from the cable. The field used (4.47 T) was the maximum field on the cable in the spot heater segment at 13 kA. The temperature used (10 K) is supposed to be the maximum temperature under the spot heater, assuming that the difference between the sensor and the hot spot is 2.3 K. The critical current was scaled by 83% in order to take into account the bending degradation. The expected critical current under these hypothesis was 28117 A.



**Figure 6: Temperature recorded by the sensor close to the spot heater BSH18 during measurement #3. The current was ramped (at 40 A/s) to 11 kA. Then the temperature was by small steps (about 150 mK) until the magnet quenched. The quench started from the spot heater segment. The heater power supply was left on after the quench.**

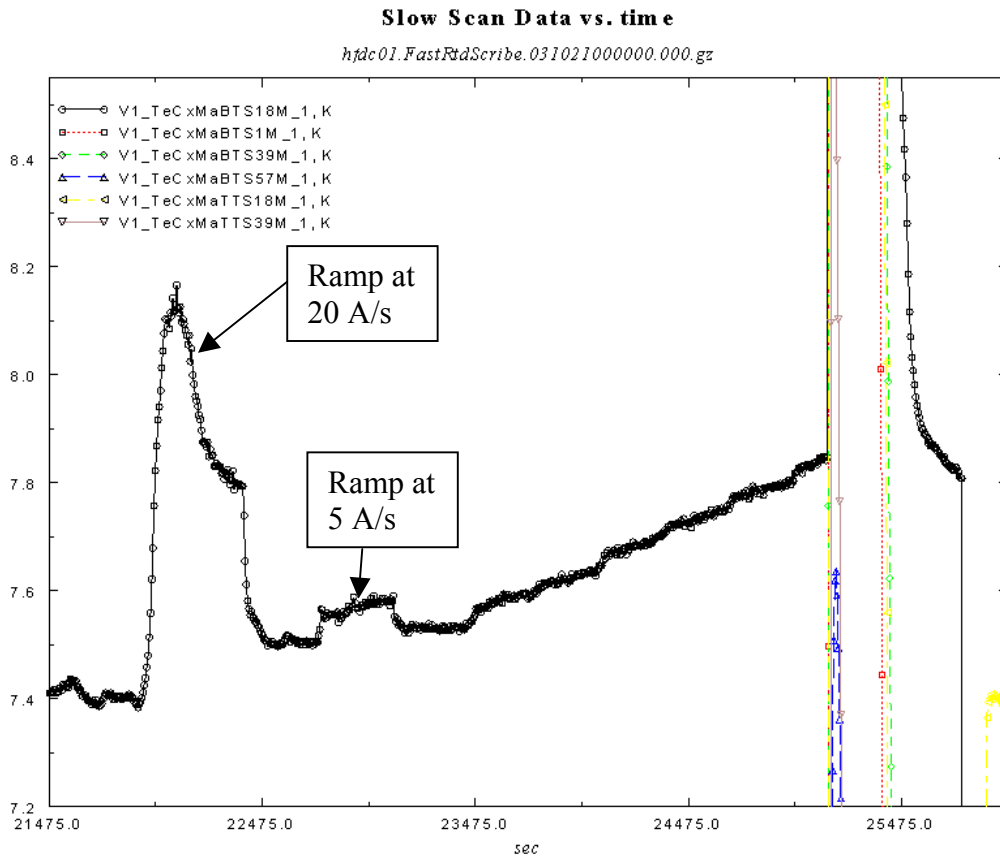


**Figure 7: Temperature recorded by the sensor close to the spot heater BSH18 during measurement #19. The temperature was raised to 7.4 K at zero current. The first pick shows the temperature increment during current ramp (at 20 A/s) to 10 kA, the second pick shows the temperature increment during ramp (at 5 A/s) to 11.5 kA. Then the temperature was slowly increased (300 mK in about 1800 sec) until the magnet quenched. The quench started from the spot heater segment.**

### HFDC-01 Quenches induced by Spot Heater

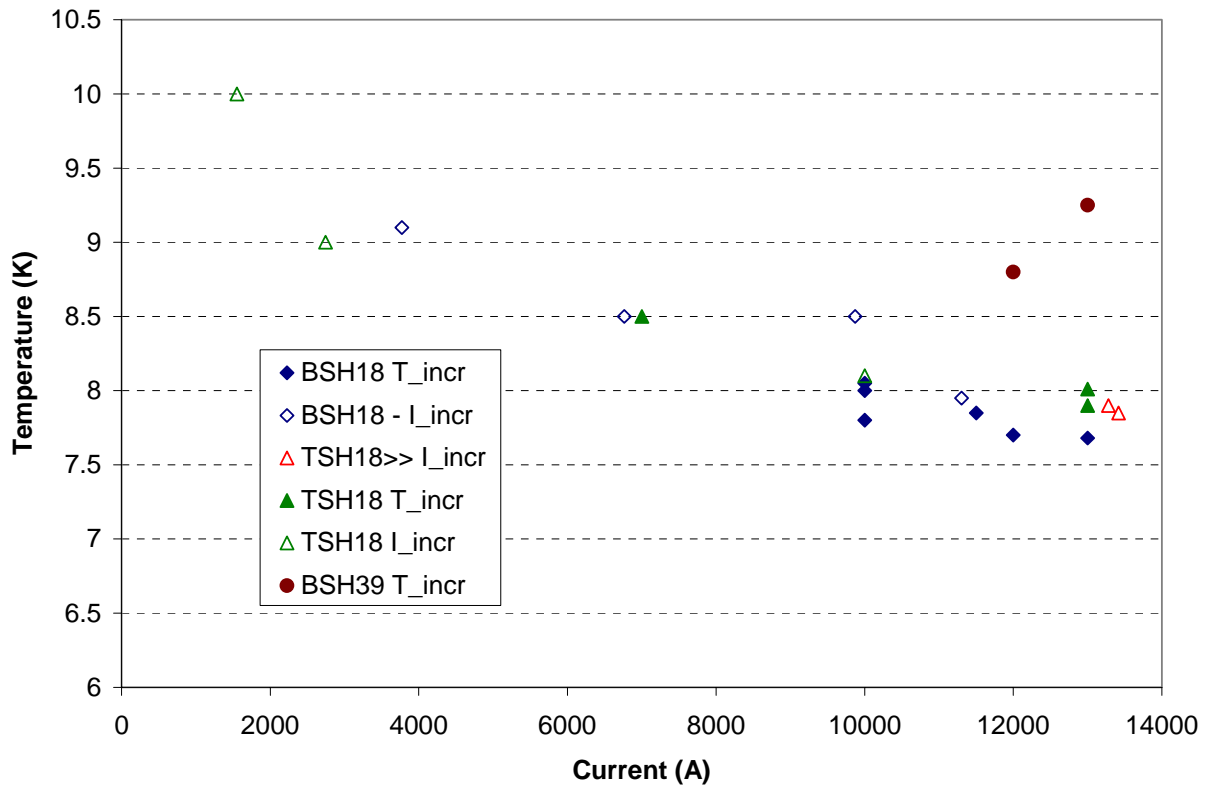


Figure 8: Temperature and current at which quenches occurred during temperature margin measurement. All results are shown in this plot.

### BSH18

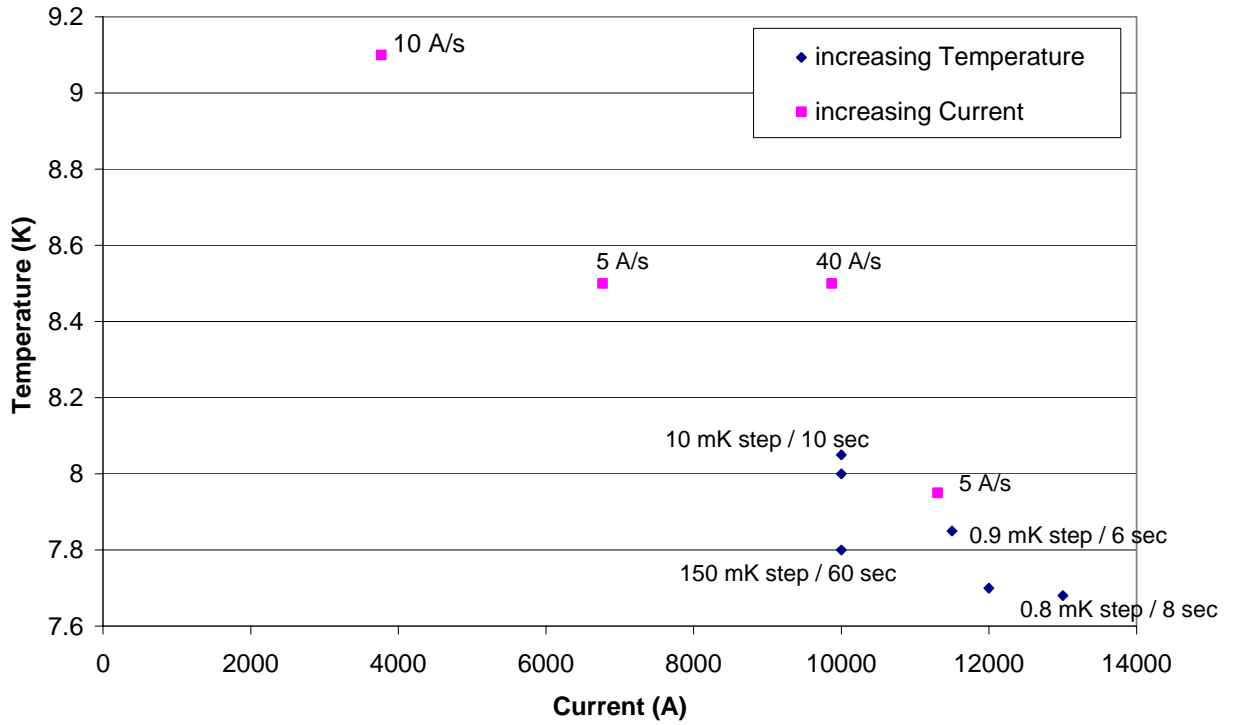


Figure 9: Temperature and current at which quenches occurred during temperature margin measurement using the Spot Heater BSH18

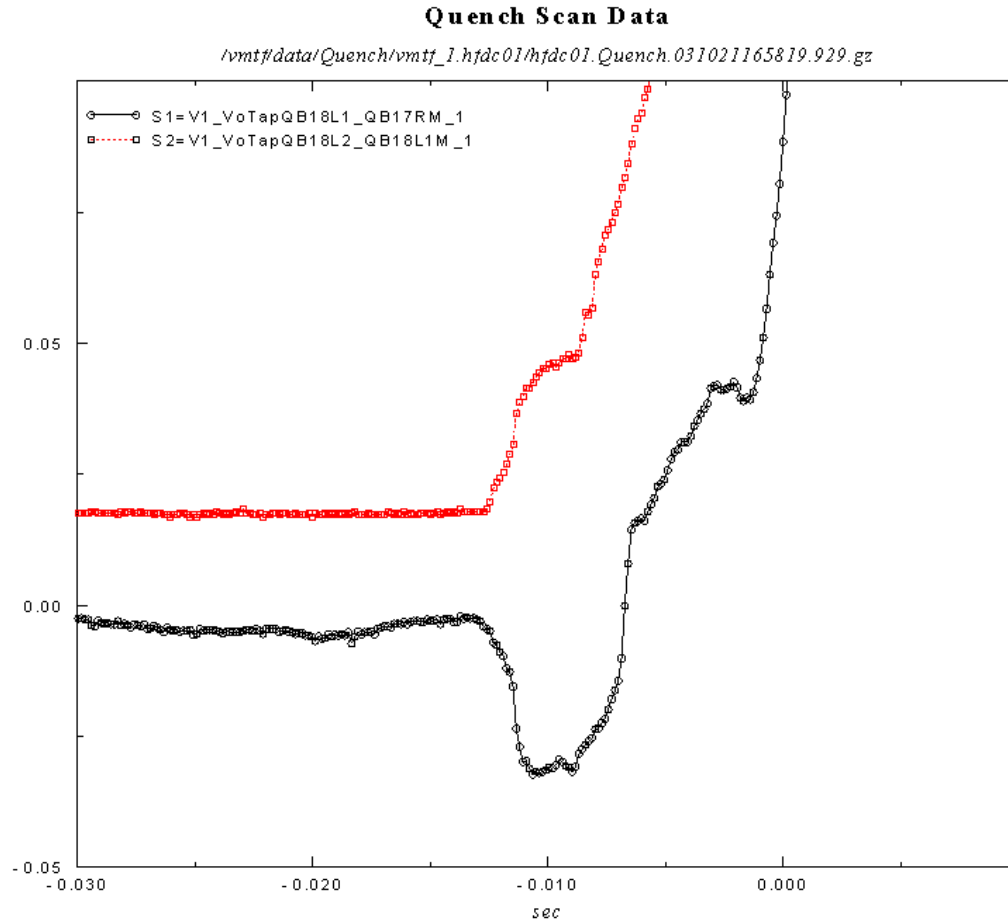


Figure 10: Voltage rise in the segment under the spot heater (red square marks) and in an adjacent segment (black circular marks). When the quench starts under the spot heater, a large negative signal is clearly visible.

## 4. Magnetic measurements in HFDC01 magnet

### 4.1 Measurement System

A vertical drive rotating coil system was used for magnetic measurements. The coil used had a nominal diameter of 2.5 cm and length 25 cm. A tangential winding measured the field harmonics; dipole windings measured the main field and allowed bucking of the large dipole component in the tangential winding signal. Coil winding voltages as well as magnet current were read by HP3458 DVMs triggered simultaneously by an angular encoder on the probe shaft to synchronize measurements of the field and the current. A centering correction was performed using feed down of higher order allowed harmonics to lower order unallowed harmonics (18, 22 pole to 16, 20 pole).

The field in the magnet body was represented in terms of harmonic coefficients defined by the power series expansion:

$$B_y + iB_x = B_1 \times 10^{-4} \sum_{n=1}^{\infty} (b_n + ia_n) \left( \frac{x + iy}{r_0} \right)^{n-1},$$

where  $B_x$  and  $B_y$  are horizontal and vertical transverse field components,  $B_1$  is the dipole field strength, and  $b_n$  and  $a_n$  are the  $2n$ -pole coefficients ( $b_1=10^4$ ) at a reference radius  $r_0$ .

A right-hand Cartesian coordinate system was defined with the  $Z$ -axis at the center of the magnet aperture, pointing from return to lead end, the  $Y$ -axis coinciding with the dipole field vector. In this paper field harmonics are presented at the reference radius of 10 mm, and  $Z = 0$  mm corresponds to the magnet physical center.

## **4.2 Measurement Results**

The model was tested in boiling liquid helium at 4.5 K at Fermilab's Vertical Magnet Test Facility. The maximum current achieved after a long training was ~13.7 kA (~5.9 T in the aperture), which is ~60% of the expected magnet short sample limit. Magnetic measurements were performed in both apertures in two thermal cycles. The aperture closest to the leads is called in this note "aperture I" whereas the other one is called "aperture II". Measurements in the aperture I were performed in TC2 and measurements in the aperture II – in TC3. Apart from that, there was a set of "warm" measurements performed at 10 A current in aperture II just before TC3.

### **Z-scans**

To evaluate distribution of the harmonics along the magnet, the probe center was consequently placed at  $Z = -750, -500, -250, 0, 250, 500, 750$  mm after the ramp up to 5 kA, then up to 12 kA and back to 5 kA. Fig. 11 shows lowest order normal and skew harmonics (sextupole and skew quadrupole) along the magnet, measured in both apertures and calculated in the return end. For correct comparison, the calculated 3D harmonics were integrated over the probe length of 250 mm centered at the same  $Z$ -positions.

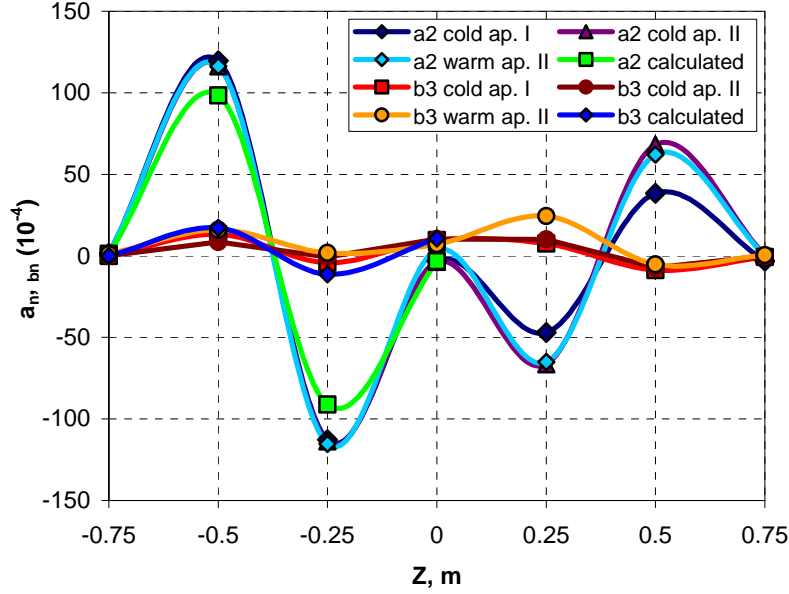


Fig. 11. Low order harmonics along the magnet.

### Geometrical Harmonics

The geometrical harmonics were determined as average values between up and down ramps at 5 kA for every Z-position. The comparison of measured and calculated in 3D case for the as-built geometry harmonics is presented in Tables II-IV. To represent the end fields, the calculated and measured harmonics were integrated for the probe placed at the longitudinal positions with  $Z = -750, -500$  and  $-250$  mm for the return end and at  $Z = 250, 500$  and  $750$  mm for the lead end and normalized to the magnetic lengths of the relevant ends.

One can see an excellent for  $Nb_3Sn$  magnet correlation between the calculated and measured harmonics in the magnet body. The integrated harmonics in the magnet return end are also consistent with the calculations. Field calculations in the magnet lead end were not done up to date, but are foreseen in the future. These results confirm high efficiency of the coil support structure for maintaining the nominal coil geometry and thus the field quality during magnet assembly and operation.

TABLE II  
[1] GEOMETRICAL HARMONICS IN MAGNET BODY

| N | Calculated "as built" values |        | Measured in aperture I            |       | Measured in aperture II |       |
|---|------------------------------|--------|-----------------------------------|-------|-------------------------|-------|
|   | $a_n$                        | $b_n$  | $a_n$                             | $b_n$ | $a_n$                   | $b_n$ |
| 2 | -3.298                       | -      | -3.28                             | 0.16  | -3.57                   | -1.26 |
| 3 | -                            | 10.638 | 0.23                              | 10.30 | -0.20                   | 10.37 |
| 4 | 0.034                        | -      | -0.35                             | 0.02  | -0.66                   | -0.17 |
| 5 | -                            | 0.353  | 0.04                              | 0.73  | -0.04                   | 0.79  |
| 6 | -0.040                       | -      | 0.00                              | -0.01 | 0.01                    | 0.01  |
| 7 | -                            | -0.083 | 0.00                              | -0.06 | -0.00                   | -0.05 |
| 8 | -0.003                       | -      | used for the centering correction |       |                         |       |
| 9 | -                            | -0.008 | -0.00                             | -0.03 | -0.00                   | -0.03 |

[2] TABLE III

[3] INTEGRATED GEOMETRICAL HARMONICS IN MAGNET RETURN END

| n | Calculated "as built" values |        | Measured in aperture I            |       | Measured in aperture II |       |
|---|------------------------------|--------|-----------------------------------|-------|-------------------------|-------|
|   | $a_n$                        | $b_n$  | $a_n$                             | $b_n$ | $a_n$                   | $b_n$ |
| 2 | 9.164                        | -      | 9.22                              | 5.26  | 3.55                    | -7.52 |
| 3 | -                            | 6.657  | -0.27                             | 9.80  | 1.01                    | 9.35  |
| 4 | 1.866                        | -      | 1.18                              | -0.06 | 0.98                    | -0.22 |
| 5 | -                            | -0.068 | 0.04                              | 0.07  | -0.02                   | -0.05 |
| 6 | 0.158                        | -      | 0.24                              | 0.01  | 0.27                    | -0.01 |
| 7 | -                            | -0.005 | -0.01                             | 0.03  | 0.01                    | 0.06  |
| 8 | -0.006                       | -      | used for the centering correction |       |                         |       |
| 9 | -                            | -0.006 | -0.00                             | -0.02 | -0.00                   | -0.02 |

[4]

[5] TABLE IV

[6] INTEGRATED GEOMETRICAL HARMONICS IN MAGNET LEAD END

| n | Measured in aperture I            |       | Measured in aperture II |       |
|---|-----------------------------------|-------|-------------------------|-------|
|   | $a_n$                             | $b_n$ | $a_n$                   | $b_n$ |
| 2 | -17.03                            | -3.04 | 2.95                    | 10.35 |
| 3 | -0.18                             | -2.38 | 2.45                    | 4.46  |
| 4 | 3.27                              | -0.10 | 2.75                    | -0.46 |
| 5 | -0.12                             | 0.06  | 0.05                    | -0.06 |
| 6 | 0.25                              | -0.03 | 0.28                    | 0.02  |
| 7 | -0.00                             | 0.05  | -0.00                   | 0.03  |
| 8 | used for the centering correction |       |                         |       |
| 9 | 0.00                              | -0.01 | -0.00                   | -0.02 |

### **Iron Saturation**

The transfer function and skew quadrupole measured in 0-12-0 kA current cycle in the magnet body and calculated in both 2D and 3D cases are shown in Fig. 2-3. The calculated in 3D case values were integrated over 250 mm region centered at  $Z = 0$  for correct comparison with the measurements.

The iron saturation effect is clear seen in both plots for the fields above 2.5 T. This effect leads to a deviation of the transfer function by 3.5% and skew quadrupole by 13 units at 5 T with respect to the 2D values. The calculated 3D values match the measurements very well for the fields above 1.5 T.

Comparison of the 2D and 3D calculations with the magnetic measurements suggests that the magnet model is too short that requires 3D magnetic analysis for proper evaluation of the field quality and transfer function.

Although the high field level, where the iron saturation play an important role, was not achieved in the model, the good correlation of measurements with the 3D calculations proves that the iron saturation effect can be accurately predicted and optimized in numerical simulations for this type of the magnet.

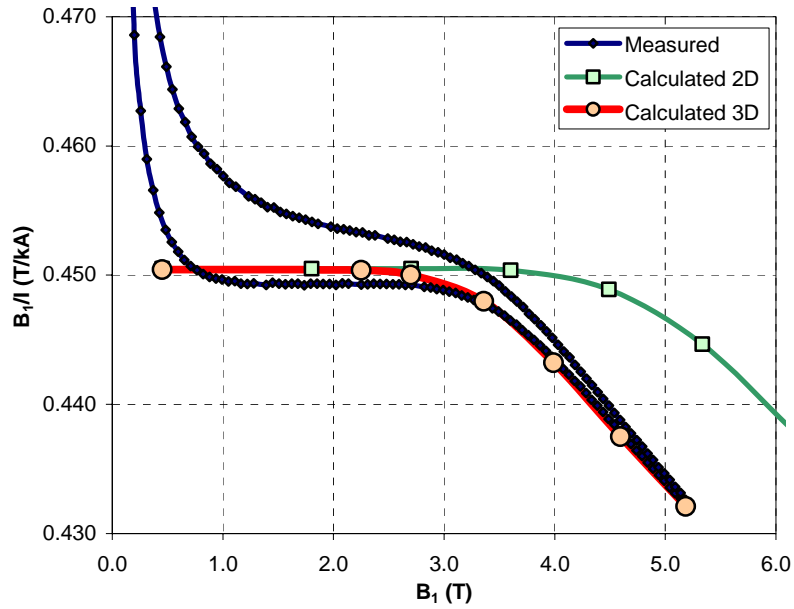


Fig. 12. Transfer function in the magnet body.

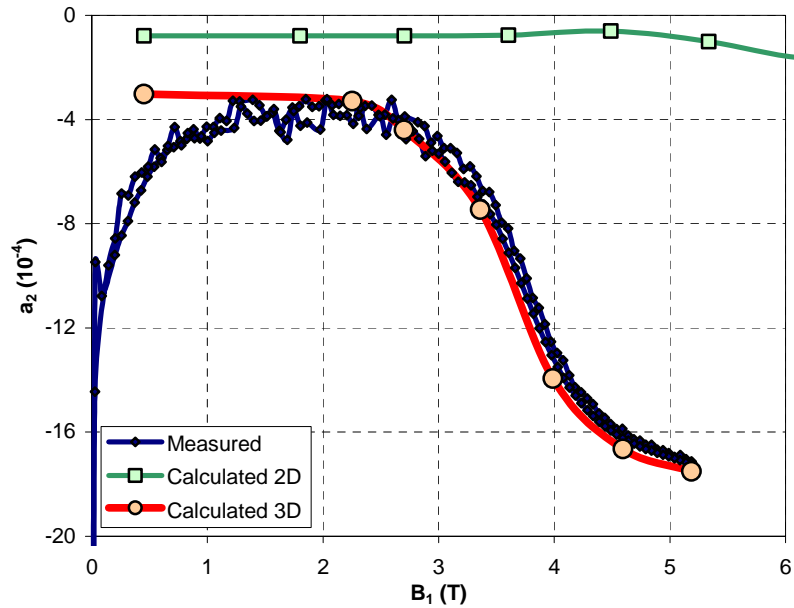


Fig. 13. Skew quadrupole in the magnet body.

### Coil Magnetization

The effect of coil magnetization on the normal sextupole measured and calculated in the magnet body is shown in Fig. 14 (the geometrical components reported in Table II were subtracted from the presented data). The up-ramp branches of both measured and calculated curves match well at the fields above 2 T. The discrepancy in the down-ramp branches at higher fields is due to superconductor re-magnetization not included in the calculation model.

One can clearly see the iron saturation effect in both loops, which would otherwise be symmetric with respect to the horizontal axis. Due to the peculiarities of magnetization flux distribution in the single-layer magnet design [1], the widths of the calculated and measured loops in Fig. 14 is a factor of 5 smaller than in the cos-theta Nb<sub>3</sub>Sn dipole models tested earlier [2] in spite of larger coil cross-section area in the common coil magnet.

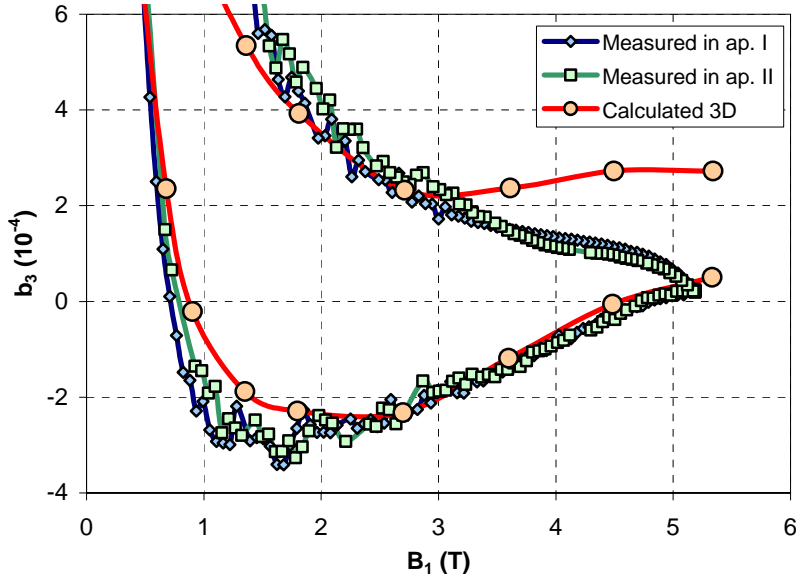


Fig. 14. Sextupole hysteresis in 0-12-0 kA cycle.

### ***Harmonics Decay and “Snapback”***

To evaluate the dynamic effects at injection-like conditions, the field measurements were performed at the current plateau of 2.4 kA during 30 minutes, following conditioning pre-cycle up to 12 kA. Measured time dependences of the skew quadrupole and sextupole at the current plateau are presented in Fig. 15.

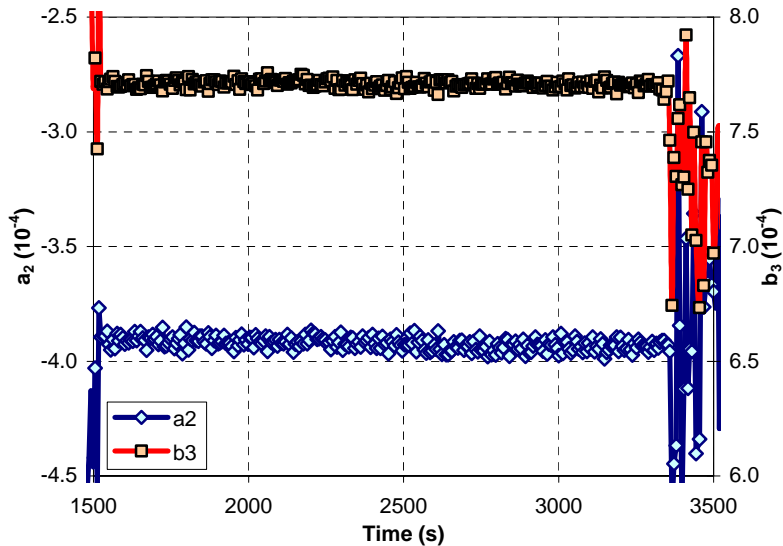


Fig. 15. Skew quadrupole and sextupole at 2.4 kA plateau.

Changes in harmonics on the current plateau were very small (less than 0.3 unit) with respect to those observed in most of NbTi accelerator magnets. This result agrees well with similar measurements of dynamic effects in Fermilab Nb<sub>3</sub>Sn cos-theta dipole models [2] and LBNL Nb<sub>3</sub>Sn common coil dipole model [3].

### **Eddy Currents**

The harmonic ramp-rate dependence was measured in three consequent current cycles up to 12 kA with the current ramp rates of 20 A/s, 40 A/s and 80 A/s. Fig. 16 shows the measured sextupole loops. It can be seen that the dependence of the sextupole on the current ramp rate is very small, which is also the case for all other harmonics. This result is consistent with a small ramp-rate dependence of AC losses measured in this model. Absence of the eddy currents in the cable is related to the quite high inter-strand resistance, created during the cable reaction with synthetic oil without transverse pressure on the cable [4].

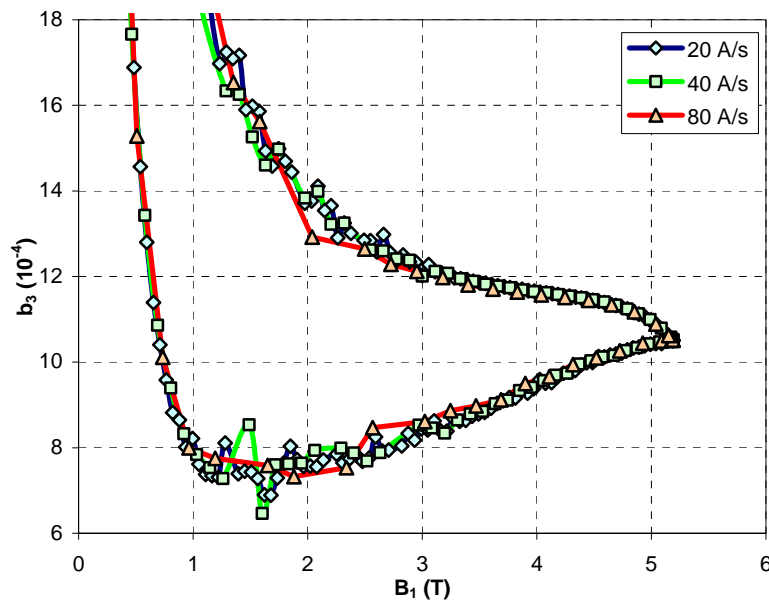


Fig. 16. Measured sextupole hysteresis at different current ramp rates.

### **4.3 Conclusion**

Magnetic field measurements were performed in both apertures of HFDC01 magnet. Due to the quench performance, the maximum current during the measurements was 12 kA. In spite of this restriction, most important effects including iron saturation were evaluated.

Field quality measurements are in an excellent agreement with the 3D magnetic analysis based on the as-built coil geometry. It confirms that the mechanical support structure of this model has higher efficiency and accuracy than support structures used in other common coil magnet designs [3].

Low coil magnetization effect is consistent with the predictions for this magnet design. If necessary, additional correction can be provided using simple and effective technique based on thin iron shims [5].

Measured field decay and “snap-back” effects are small. Virtual absence of the dynamic effects in the field quality, observed in this model and in few previously tested Nb<sub>3</sub>Sn shell-type dipole magnets is an exciting result that may essentially simplify a field correction system and operation of future hadron colliders utilizing high field Nb<sub>3</sub>Sn magnets.

### 3.4 REFERENCES

- [7] V.V. Kashikhin, A.V. Zlobin, “Correction of the persistent current effect in Nb<sub>3</sub>Sn dipole magnets”, *Proc. ASC2000, IEEE Trans. Applied Superconductivity*, Vol. 11, No. 1, March 2001, pp.2058-2061.
- [8] E. Barzi, R. Carcagno, D. Chichili, J. DiMarco, H. G. Glass, V.V. Kashikhin, M. Lamm, J. Nogiec, D. Orris, T. Peterson, R. Rabehl, P. Schlabach, C. Sylvester, M. Tartaglia, J.C. Tompkins, G. Velev, A.V. Zlobin, “Field Quality of the Fermilab Nb<sub>3</sub>Sn Cos-theta Dipole Models”, *Proc. EPAC2002*, June 2002, pp.2403-2405.
- [9] A.F Leitzke, S. Caspi, L. Chiesa, M. Coccoli, D.R. Dietderich, P. Ferracin, S.A. Gourlay, R.R. Hafalia, A.D. McInturff, G. Sabbi, R.M. Scanlan, “Test results of RD3c, A Nb<sub>3</sub>Sn common-coil racetrack dipole magnet”, *Proc. ASC2002, IEEE Trans. Applied Superconductivity*, Vol. 13, No. 2, June 2003, pp.1292-1296.
- [10] G. Ambrosio, E. Barzi, D. Chichili, L. Elementi, A.V. Zlobin, “Measurement of Inter-Strand Contact Resistance in Epoxy Impregnated Nb<sub>3</sub>Sn Rutherford Cables”, *Proc. CEC/ICMC-2003*, Anchorage, Alaska, September 22-25, 2003.
- [11] E. Barzi, D. Chichili, J. DiMarco, V.V. Kashikhin, M. Lamm, P. Schlabach, A.V. Zlobin, “Passive correction of the persistent current effect in Nb<sub>3</sub>Sn accelerator magnets”, *Proc. ASC2002, IEEE Trans. Applied Superconductivity*, Vol. 13, No. 2, June 2003, pp.1270-1273.

## 5. Strain gauge results

Two sets of data, which correspond of to two loading lines (see Fig. 17), are presented.

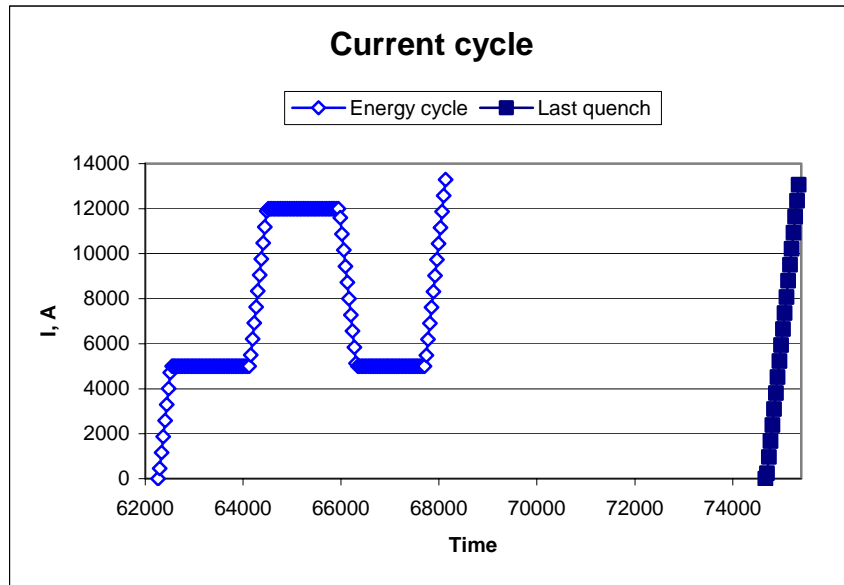


Figure. 17 Current loading lines.

### Bullet Gauge Data:

Total sixteen bullets were installed in the magnet see Fig. X, eight per end.

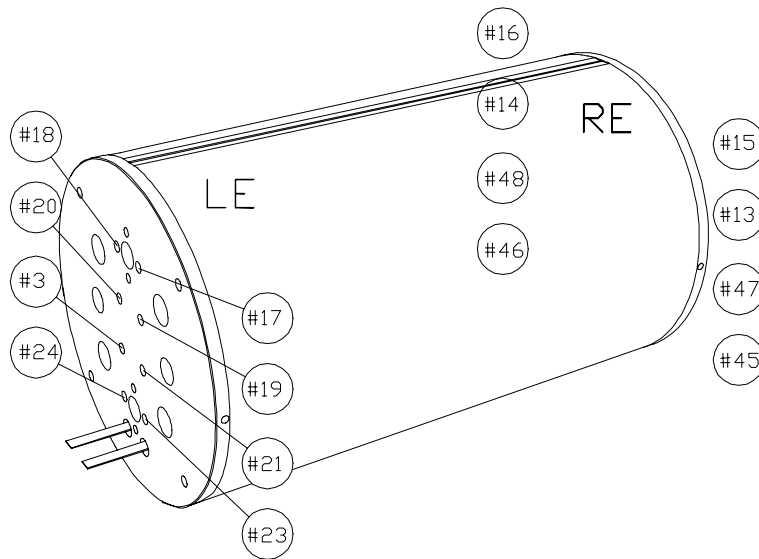


Figure 18. Bullet map for the Common Coil Magnet.

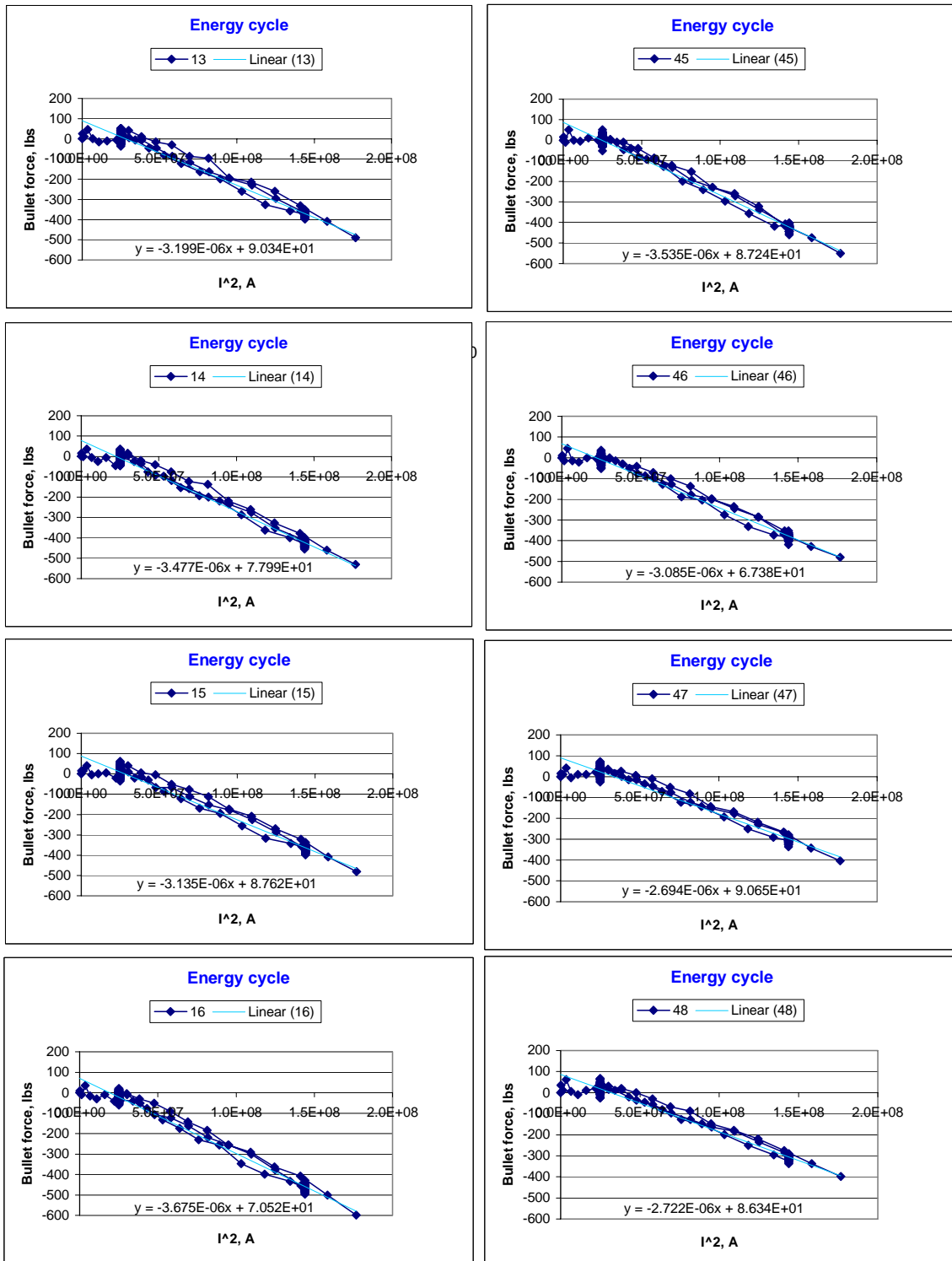


Figure 19. Behavior of RE bullets during “energy cycle”.

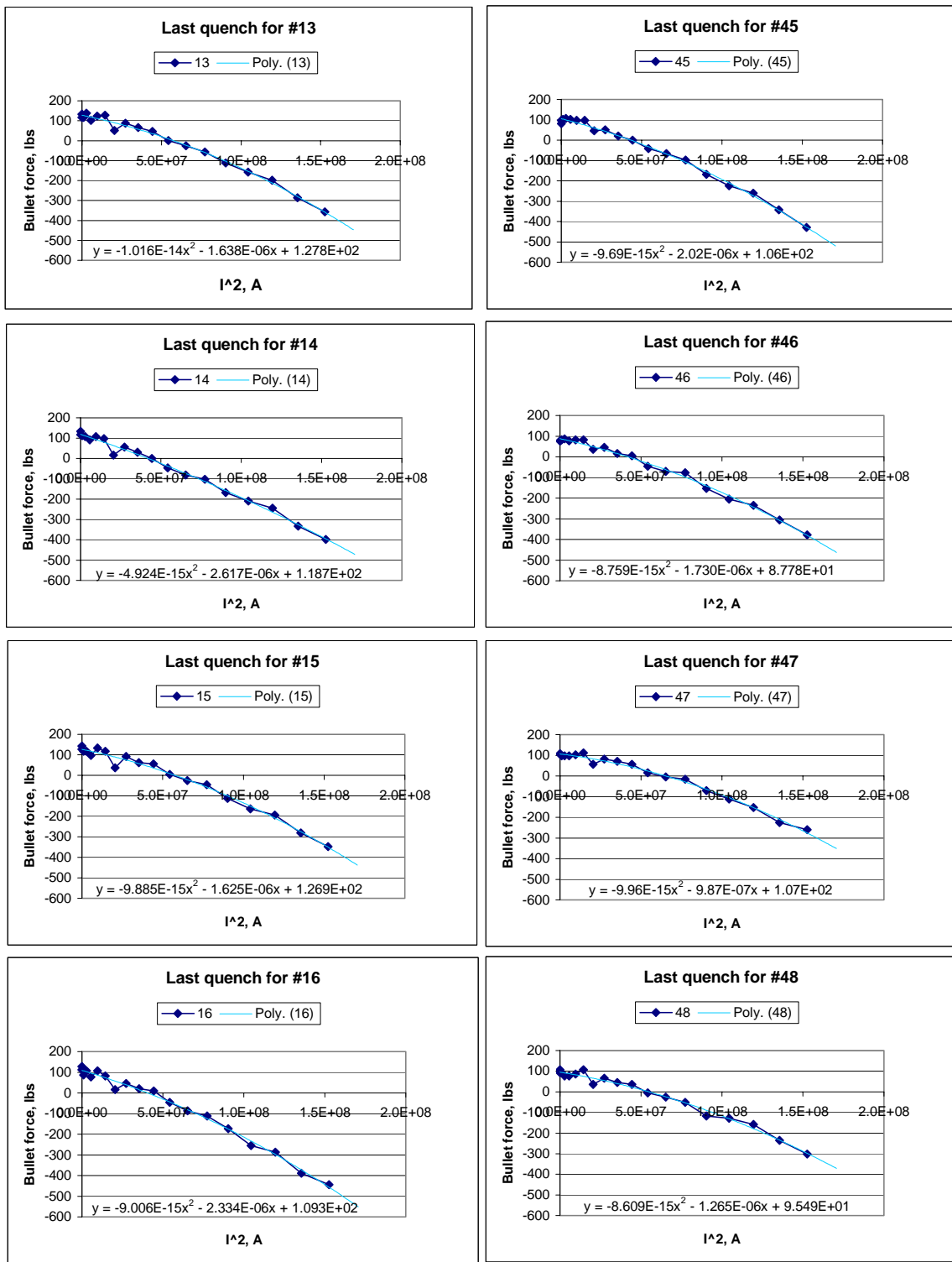


Figure 20. Behavior of RE bullets during “last quench”.

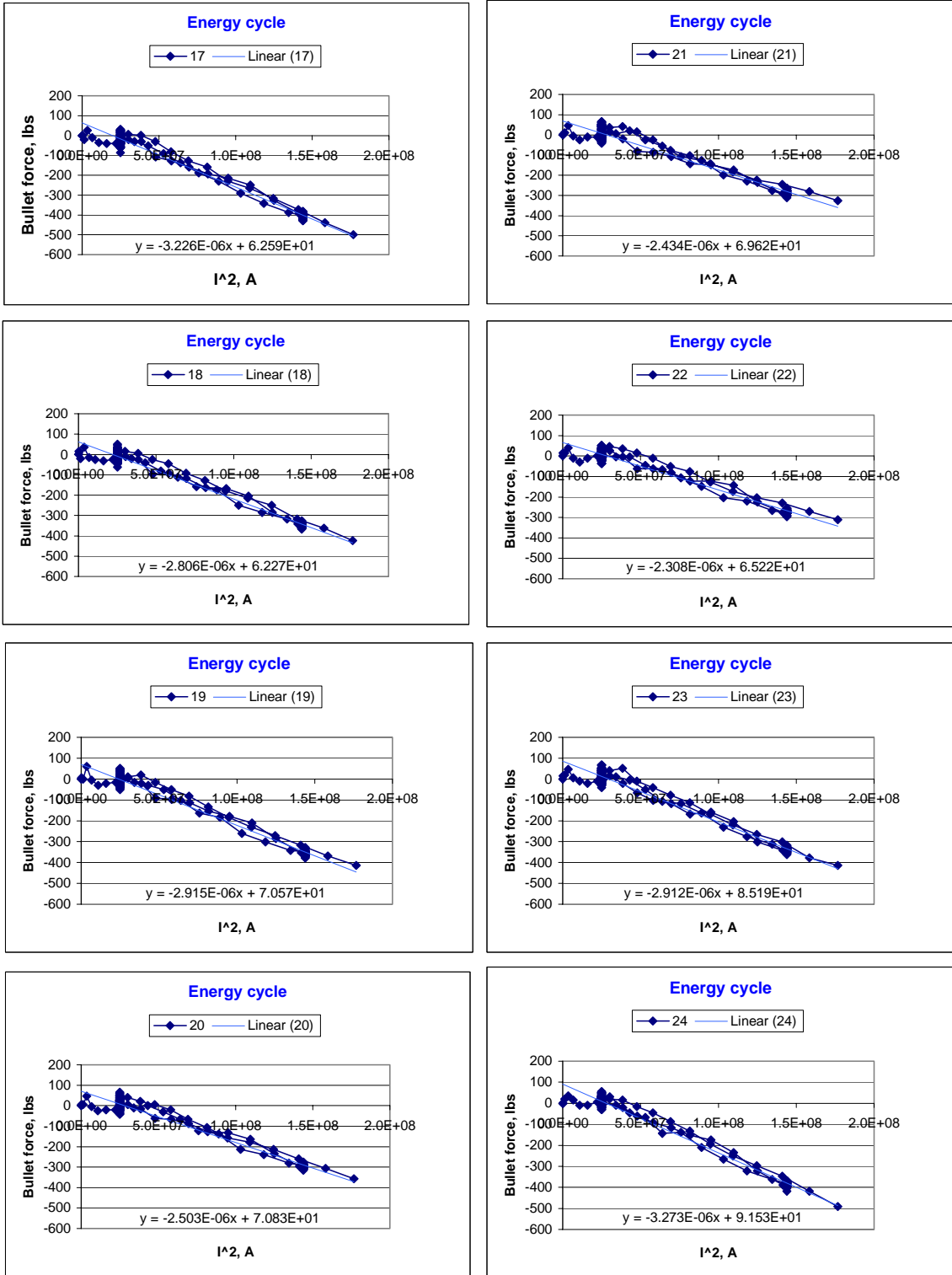


Figure 20. Behavior of RE bullets during “energy cycle”.

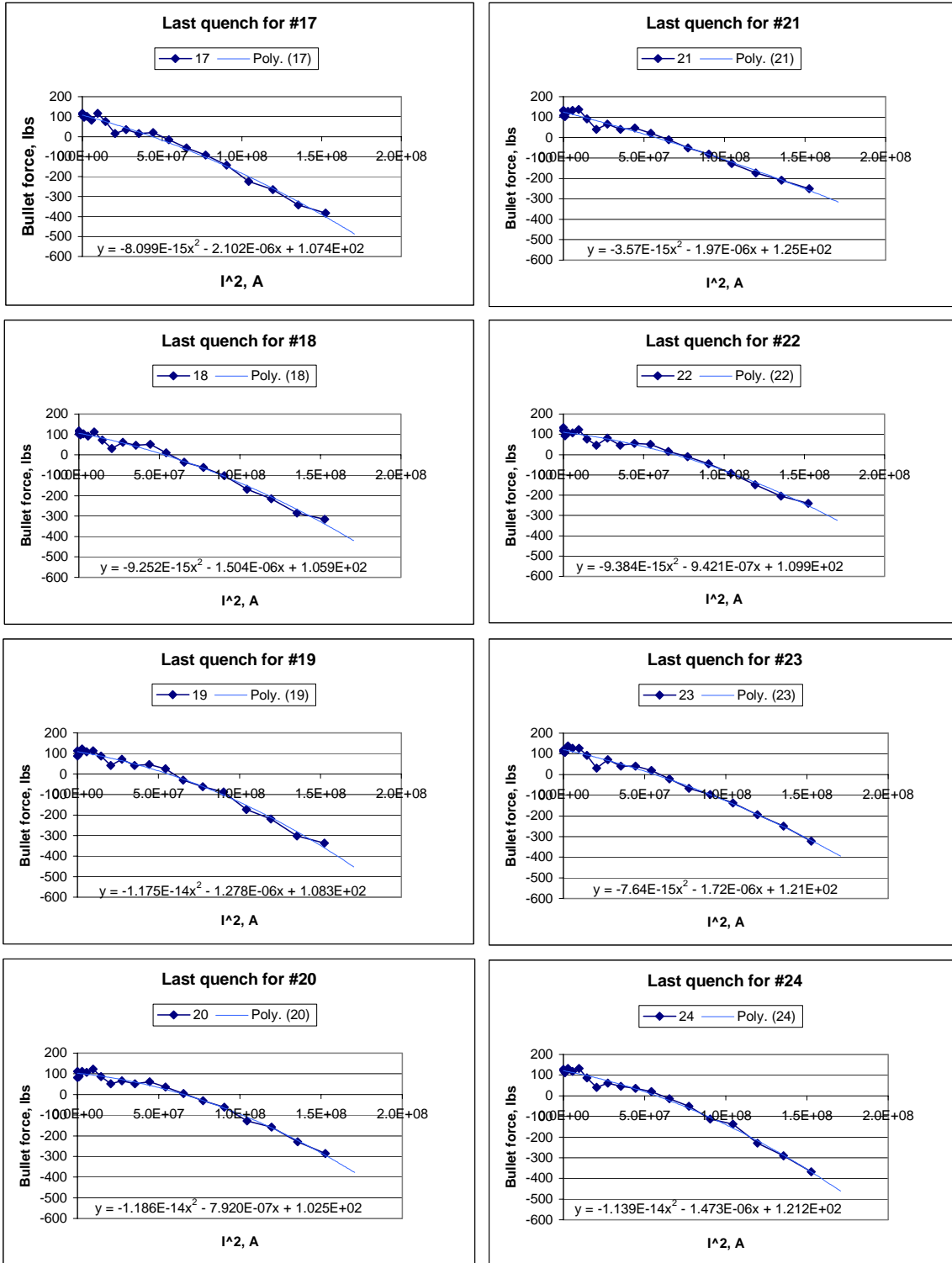


Figure 21. Behavior of RE bullets during “last quench”.

### Skin Strain Gauge Data

Strain gauges were mounted on the magnet skin to measure azimuthal stress near the mid-plane ( $30^\circ$ -SG2b,SG4b) and at pole region ( $60^\circ$ -SG2a, SG4a) at two cross-sections: the middle of the magnet (SG4) and near the transition area (SG2). Longitudinal stress distribution measured by gauges SG1-SG7 located at  $90^\circ$  relative to magnet pole plane.

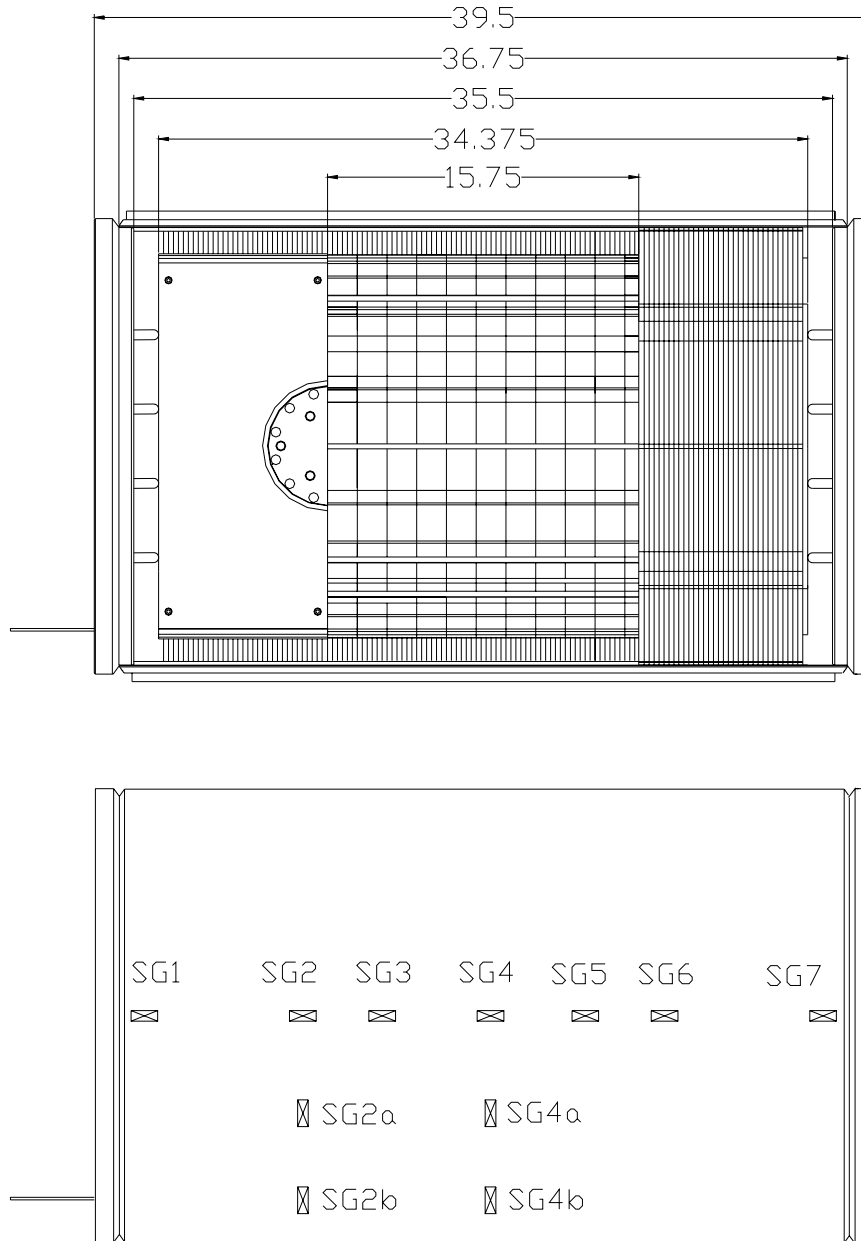


Fig. 22: Map of Skin Gauges for the Common Coil Magnet.

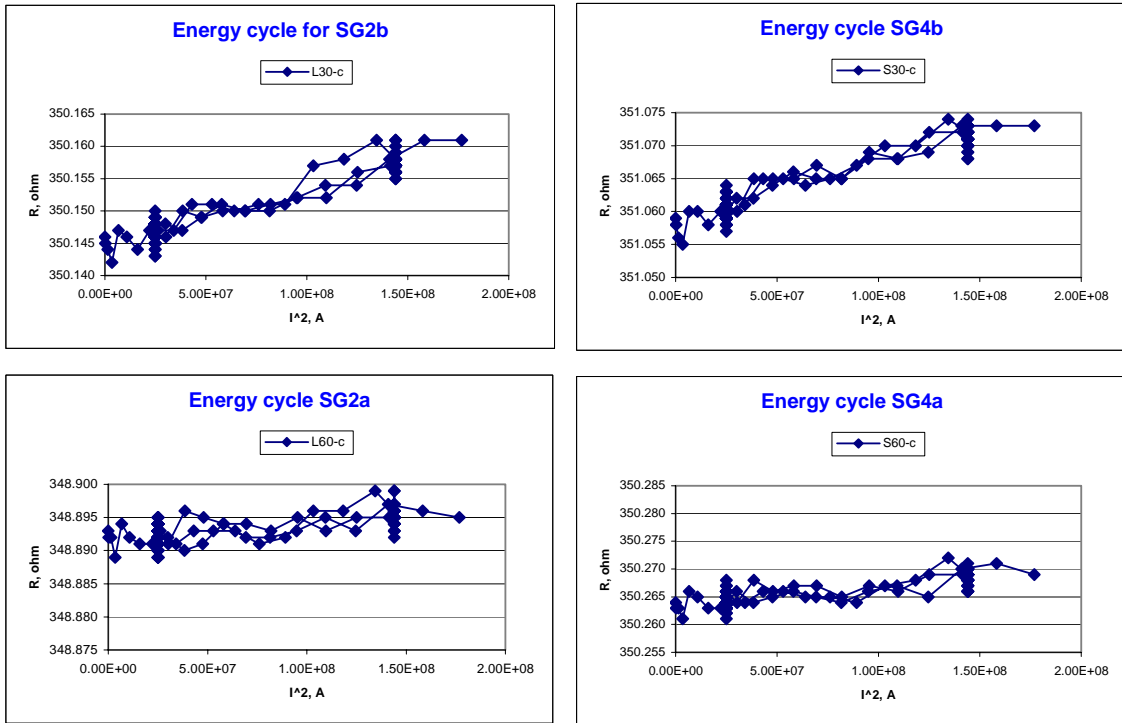


Figure 23. Azimuthal gauge data during "energy cycles".

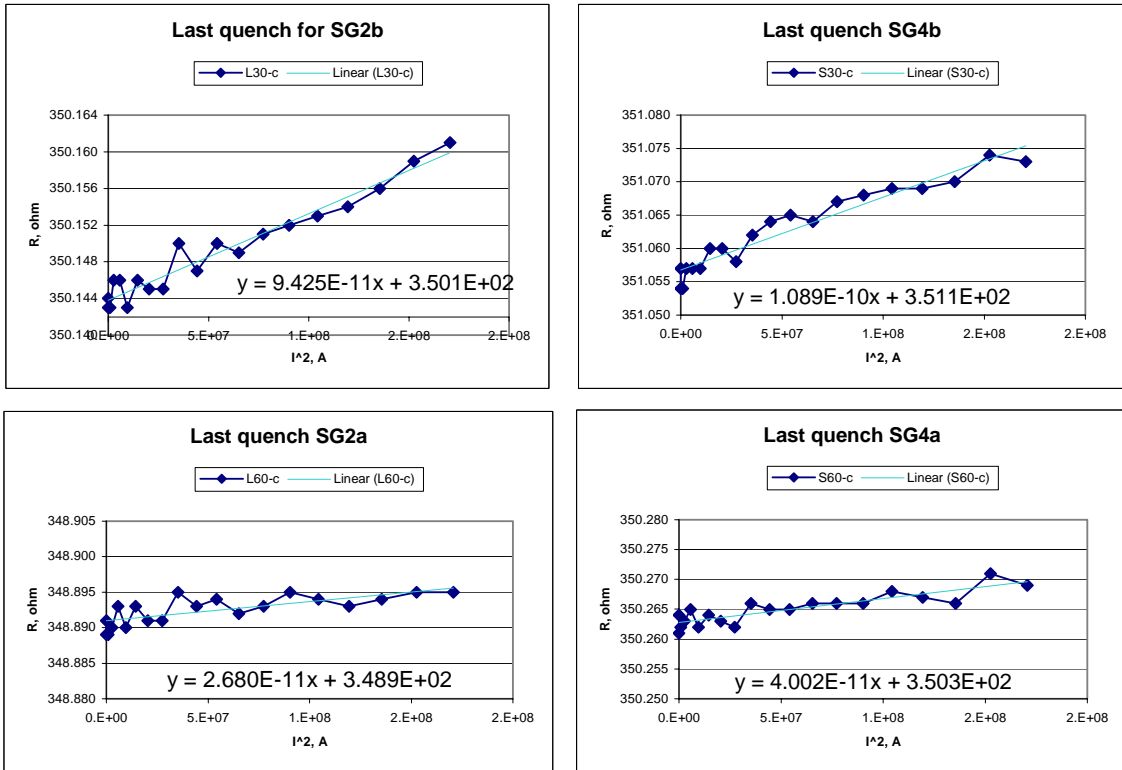


Figure 24. Azimuthal gauge data during "last quench".

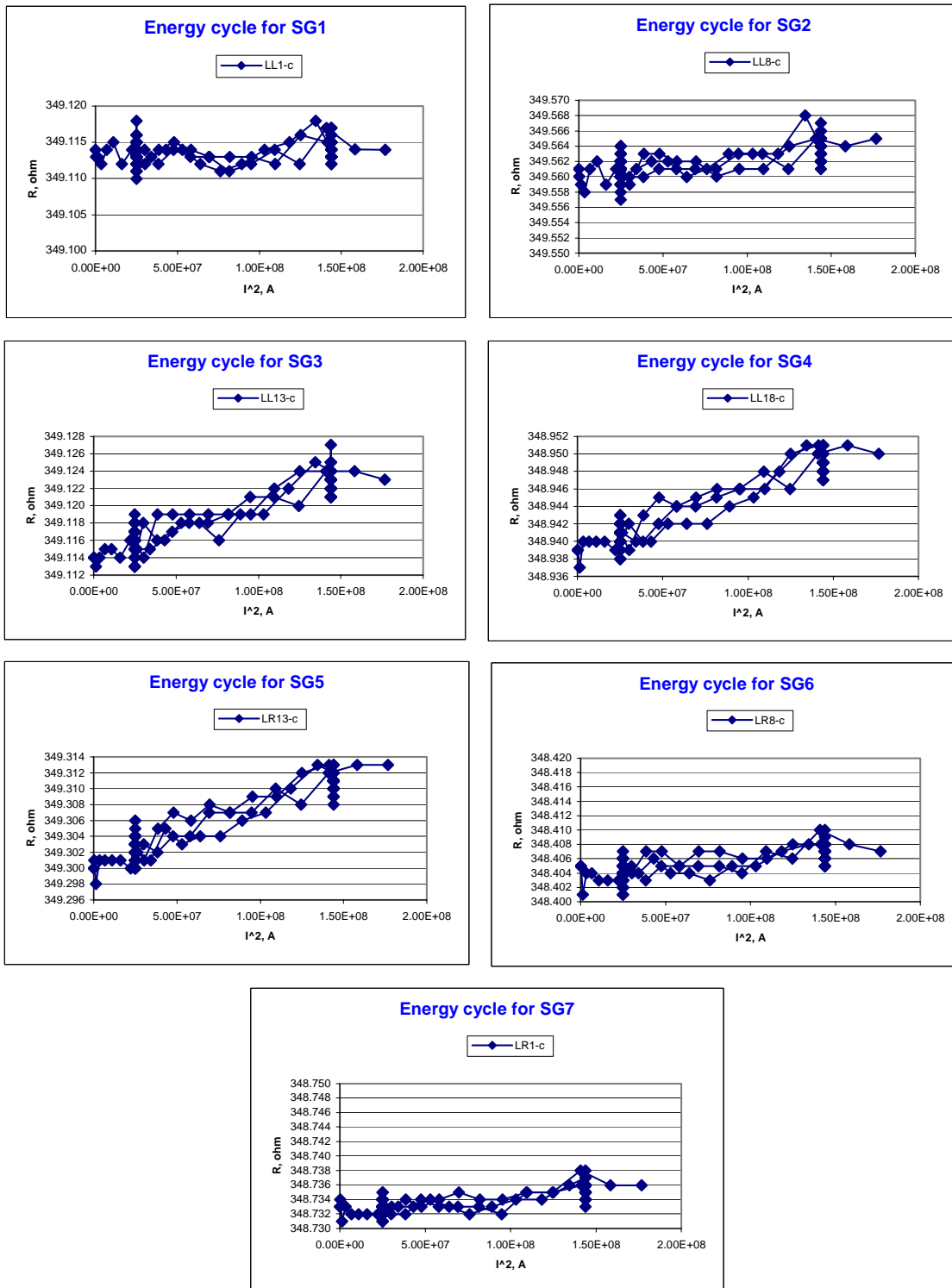


Figure 25. Longitudinal gauges data during “energy cycle”.

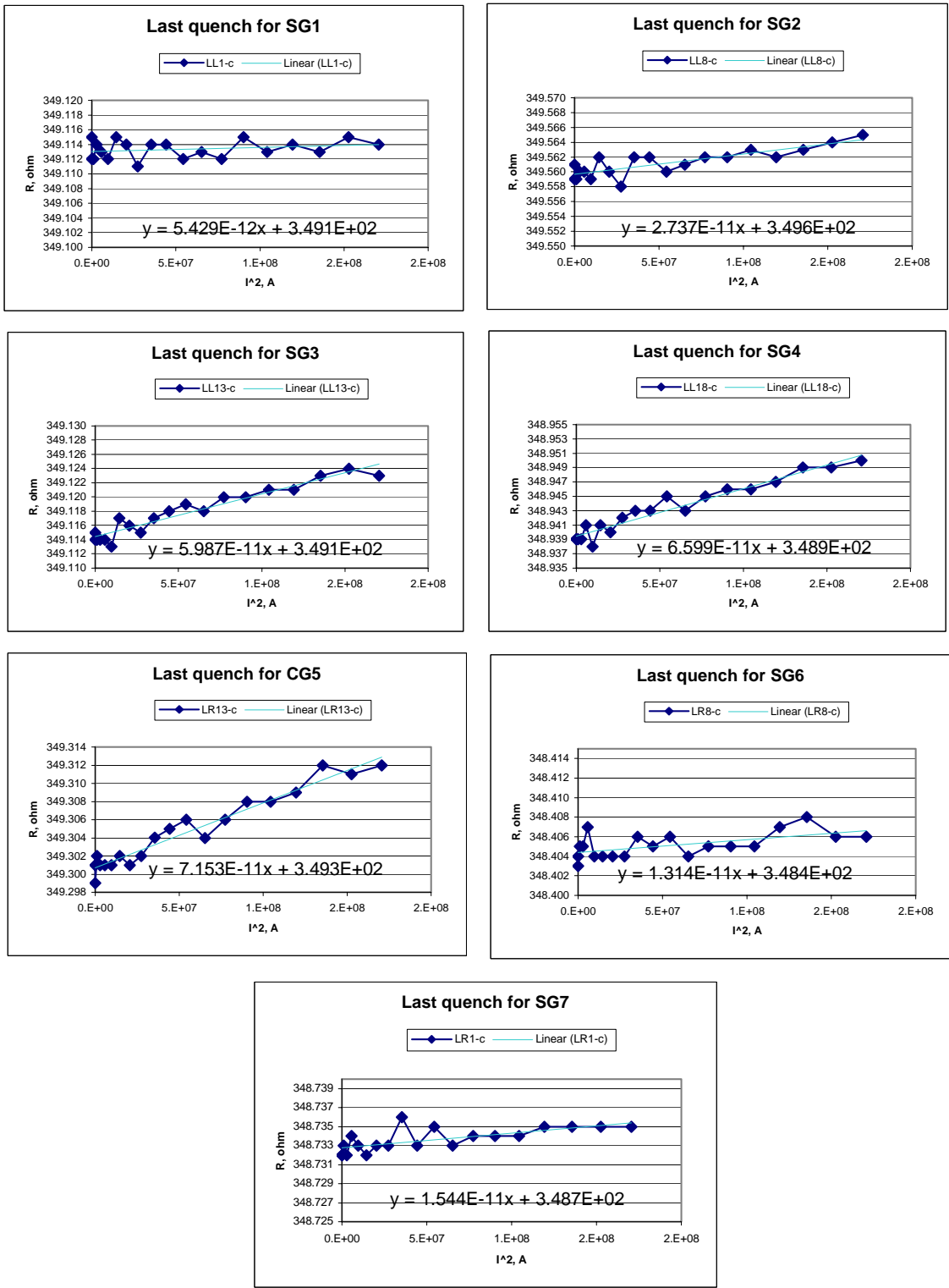


Figure 26. Longitudinal gauges data during “last quench”.

Table V. Azimuthal gauge data.

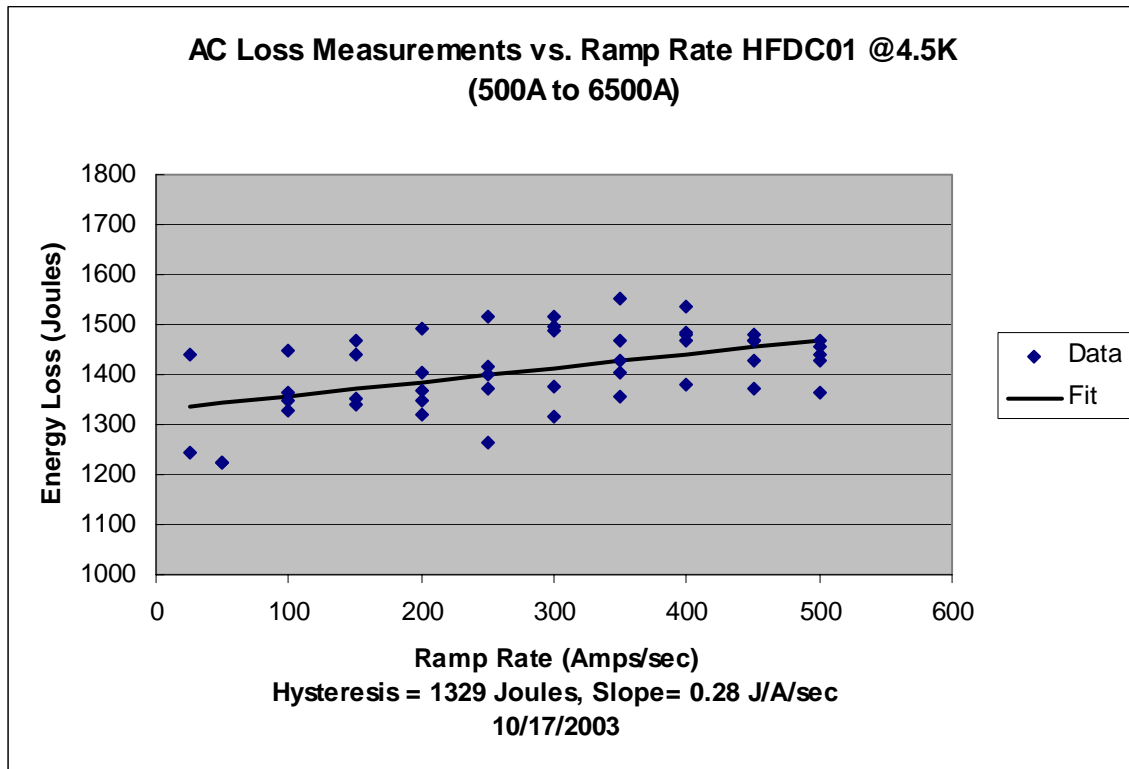
| VMTF name | IB3 name | Gage Factor | R <sub>zero</sub> | R <sub>4.2K</sub> | R <sub>final</sub> | R <sub>final-R<sub>4.2K</sub></sub> | E, GPa   | LF-Stress, MPa | Stress, MPa |
|-----------|----------|-------------|-------------------|-------------------|--------------------|-------------------------------------|----------|----------------|-------------|
| L60       | SG2A     | 2.03        | 348.97049         | 348.891           | 348.895            | 0.004                               | 2.15E+11 | 1.2            | -22.9       |
| L30       | SG2B     | 2.03        | 348.961           | 350.1438          | 350.16             | 0.0162                              | 2.15E+11 | 4.9            | 363.9       |
| S60       | SG4A     | 2.03        | 349.05151         | 350.2628          | 350.27             | 0.0072                              | 2.15E+11 | 2.2            | 369.7       |
| S30       | SG4B     | 2.03        | 348.88501         | 351.0568          | 351.075            | 0.0182                              | 2.15E+11 | 5.5            | 664.8       |

Table VI. Longitudinal gauge data.

| VMTF name | IB3 name | Gage Factor | R <sub>zero</sub> | R <sub>4.2K</sub> | R <sub>final</sub> | R <sub>final-R<sub>4.2K</sub></sub> | E, GPa   | LF-Stress, MPa | A, mm <sup>2</sup> | F, N  | F, lbs |
|-----------|----------|-------------|-------------------|-------------------|--------------------|-------------------------------------|----------|----------------|--------------------|-------|--------|
| LL1       | SG1      | 2.03        | 349.04849         | 349.113           | 349.114            | 0.001                               | 2.15E+11 | 0.3            | 18000              | 5461  | 1201   |
| LL8       | SG2      | 2.03        | 348.99551         | 349.5597          | 349.565            | 0.0053                              | 2.15E+11 | 1.6            | 18000              | 28905 | 6359   |
| LL13      | SG3      | 2.03        | 348.91751         | 349.1144          | 349.125            | 0.0106                              | 2.15E+11 | 3.2            | 18000              | 57883 | 12734  |
| LL18      | SG4      | 2.03        | 348.91449         | 348.9395          | 348.95             | 0.0105                              | 2.15E+11 | 3.2            | 18000              | 57366 | 12621  |
| LR13      | SG5      | 2.03        | 349.1705          | 349.301           | 349.313            | 0.0123                              | 2.15E+11 | 3.7            | 18000              | 67131 | 14769  |
| LR8       | SG6      | 2.03        | 348.461           | 348.404           | 348.407            | 0.0026                              | 2.15E+11 | 0.8            | 18000              | 14227 | 3130   |
| LR1       | SG7      | 2.03        | 348.83402         | 348.7328          | 348.736            | 0.0032                              | 2.15E+11 | 1.0            | 18000              | 17493 | 3849   |

## 6. AC Loss Measurements

AC loss measurements were performed on magnet HFDC01 at a temperature of 4.5K. The standard ramp profile for these measurements was from 500Amps to 6500Amps and back down to 500Amps using ramp rates of 25Amps/sec up to 500 Amps/sec. All but two ramp rates were performed at the standard sample rate of 60Hz. Due to memory limitations of the AC loss measurement hardware the data was taken at a sample rate of 15Hz for ramp rates of 25Amps/sec and 50Amps/sec. The measured hysteresis for this magnet was 1324 +/- 22 Joules and the measured slope was 0.28 +/- 0.07 Joules/Amp/Sec.



## 7. RRR measurement

The RRR measurement was performed in the end of September 2003. The racetrack magnet was gradually warming up and meanwhile we recorded the whole coil voltage value generated by  $\pm 10$  A across the magnet. In figure 27 we plotted the voltage change close to the transition temperature. The measured RRR for the whole coil is 3.9. It is interesting to notice that the two half coil RRR values are different. The Top half RRR=3.5 while the Bottom coil RRR=4.6. Figure 28 and Figure 29 represent the coil segment RRR values for the Top and Bottom coils respectively.

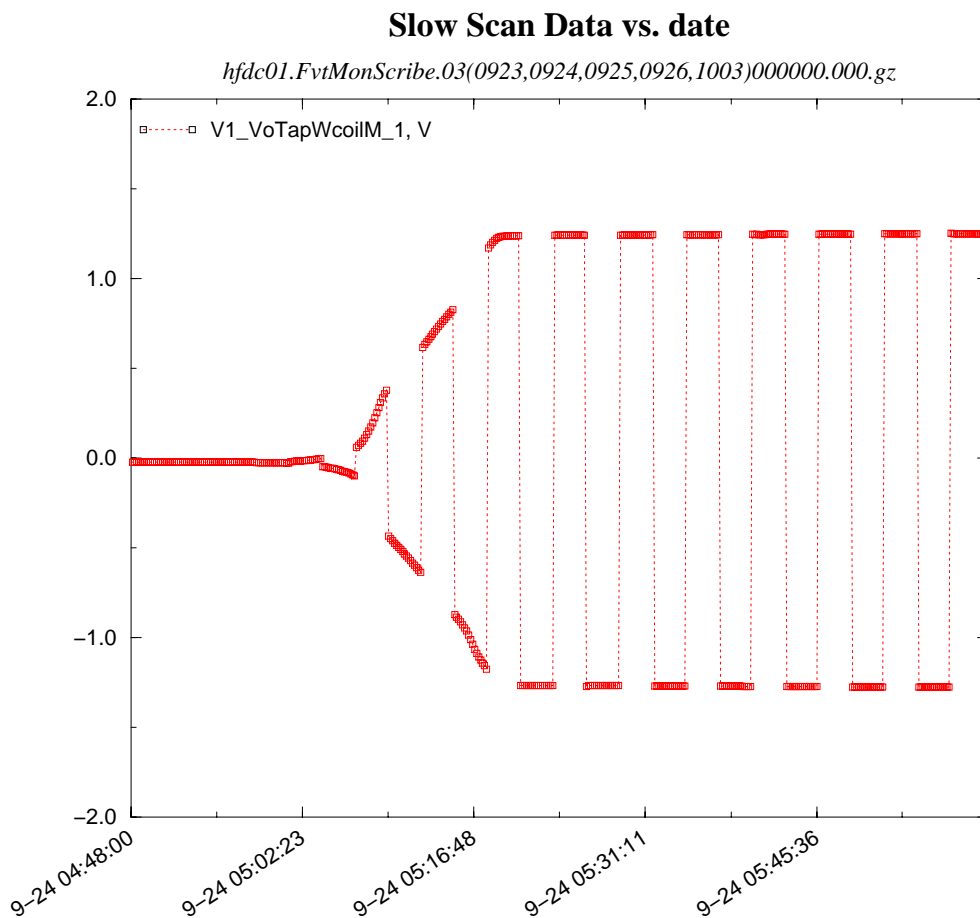


Figure 27. It shows the voltage rise of the whole coil signal at transition temperatures when  $\pm 10$  A is applied.

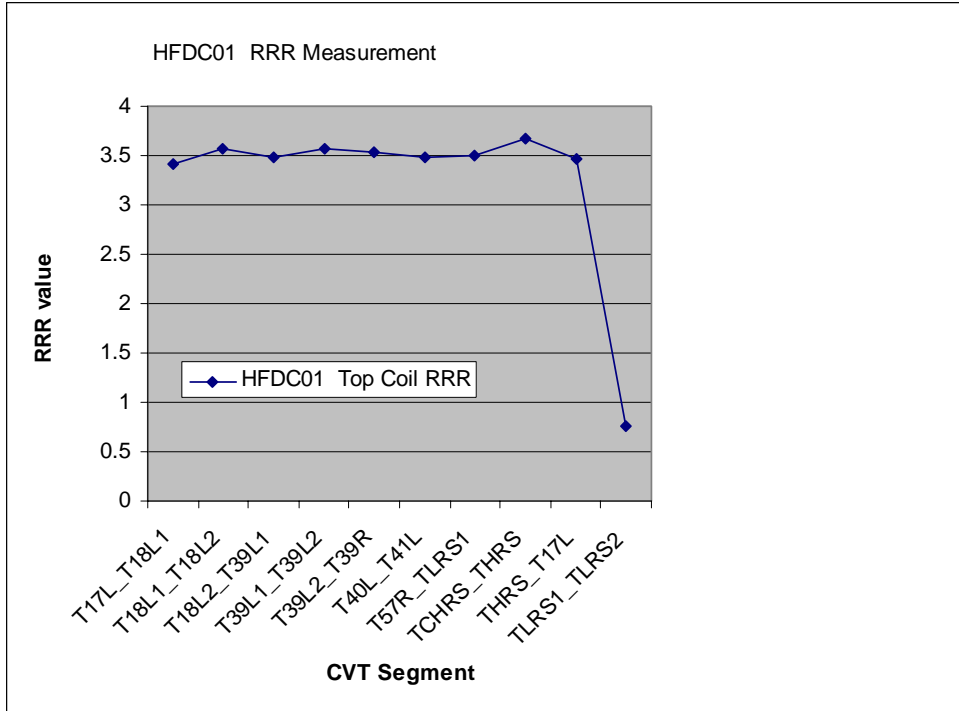


Figure 28. Top coil RRR values as a function of CVT segments.

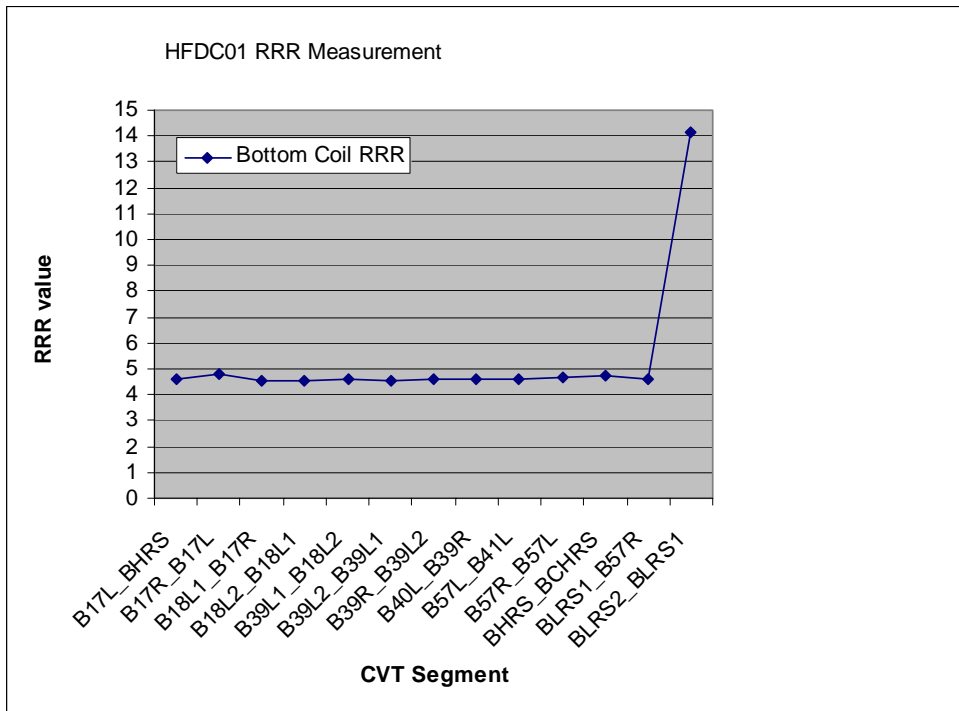


Figure 29. Bottom coil RRR values as a function of CVT segments.